# The Influence of Ring-Expanded N-Heterocyclic Carbenes on the Structures of Half-Sandwich Ni(I) Complexes: An X-Ray, EPR, and ENDOR Study

Stefan Pelties,[‡] Emma Carter,[#] Andrea Folli,[#] Mary F. Mahon,[†] Damien M. Murphy,*[,#] Michael K. Whittlesey,*[,†] and Robert Wolf*[,‡]

[‡] *Institute of Inorganic Chemistry, University of Regensburg, 93040 Regensburg, Germany*

[#] *School of Chemistry, Cardiff University, Park Place, Cardiff CF10 3AT, UK*

[†] *Department of Chemistry, University of Bath, Claverton Down, Bath BA2 7AY, UK*

**Abstract**

Potassium graphite reduction of the half-sandwich Ni(II) ring-expanded diamino/diamidocarbene complexes CpNi(RE-NHC)Br gave the Ni(I) derivatives CpNi(RE-NHC) (RE-NHC = 6-Mes (**1**), 7-Mes (**2**), 6-MesDAC (**3**)) in yields of 40-50%. The electronic structures of paramagnetic **1**-**3** were investigated by CW X-/Q-band EPR and Q-band $^{1}$H ENDOR spectroscopy. Whilst small variations in the *g* values were observed between the diaminocarbene complexes **1** and **2**, pronounced changes in the *g* values were detected between the almost isostructural **1** and diamidocarbene species **3**. These results highlight the sensitivity of the EPR **g** tensor to changes in the electronic structure of the Ni(I) centers generated by incorporation of heteroatom substituents onto the backbone ring positions. Variable temperature EPR analysis also revealed the presence of a second Ni(I) site in **3**. The experimental *g* values for these two Ni(I) sites detected by EPR in frozen solutions of **3** are consistent with resolution on the EPR timescale of the disordered components evident in the X-ray crystallographically determined structure and the corresponding DFT calculated **g** tensor. Q-band $^{1}$H ENDOR measurements revealed a small amount of unpaired electron spin density on the Cp rings, consistent with the calculated SOMO of the complexes **1**-**3**. The magnitude of the $^{1}$H *A* values for **3** were also notably larger compared to **1** and **2**, again highlighting the influence of the diamidocarbene on the electronic properties of **3**.

## Introduction

The chemistry of Ni(I) has undergone a significant resurgence in recent years. While clearly established as an oxidation state of importance in bio-inorganic chemistry,[1-12] the role of Ni(I) in homogeneous catalytic cycles has remained less clear cut.[13,14] This has now started to change thanks to the increased number of Ni(I) species that have been prepared and characterized[15-53] and, as a result, investigated in relation to catalytic,[23-29,43-45,54-61] as well as stoichiometric, transformations.[18,19,30-42] A significant portion of the very latest work has employed N-heterocyclic carbene (NHC) ligands in efforts to prepare highly reactive two- and three-coordinate Ni(I) species, a number of which are shown in Scheme 1. Thus, use of the N-aryl NHCs IMes (1,3-bis(2,4,6-trimethylphenyl)imidazol-2-ylidene) and IPr (1,3-bis(2,6-diisopropylphenyl)imidazol-2-ylidene) has allowed formation of three-coordinate bis-NHC halide complexes (**A**) with applications in catalytic C-C bond formation.[43-45] In pioneering studies, the Hillhouse group showed that IPr was sufficiently bulky to stabilize even two-coordinate mono-carbene Ni(I) complexes bearing amido, aryl and, remarkably, even alkyl ancillary ligands (**B**/**C**).[46-50] Very recently, the groups of Wolf[51,52] and Hazari[53] independently prepared a range of Cp′Ni(NHC) (Cp′ = $C_5H_5$, $C_5Me_5$ ($Cp^*$), $C_5(C_6H_4\text{-}4\text{-}Et)_5$)) complexes (**D**) and indenyl (Ind) analogues, again employing IPr and IMes (as well as the saturated derivative SIPr), via reduction of either the half-sandwich precursors Cp′Ni(NHC)Cl or treatment of the dimer $[Ni(NHC)(\mu\text{-}Cl)]_2$ with NaCp or LiInd. As an alternative to the use of bulky 5-membered ring NHCs, Whittlesey's group have employed ring-expanded NHCs (RE-NHCs), a generic name for carbene ligands based on ring sizes of 6-8,[62-69] for the synthesis of a series of Ni(RE-NHC)($PPh_3$)Br derivatives.[70-72] In the case of the 6-

membered N-mesityl (6-Mes) derivative **E**, treatment with additional 6-Mes led to formation of the highly unusual two-coordinate Ni(I) salt, [Ni(6-Mes)$_2$]Br (**F**).[73]

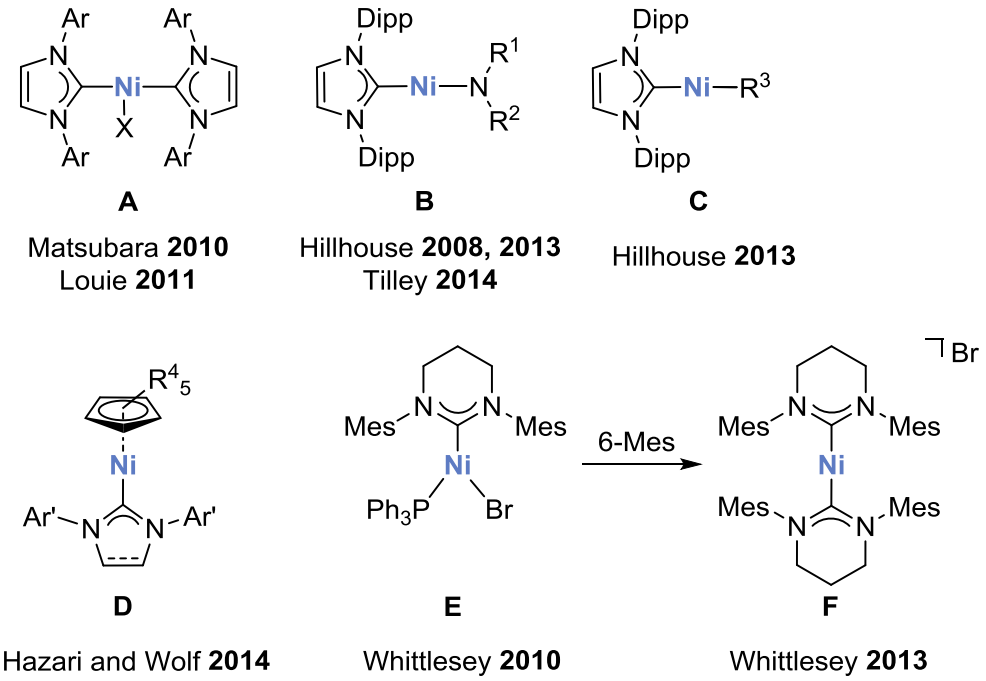


**Scheme 1.** Selected examples of mononuclear nickel(I) NHC complexes. **A**: Ar = 2,6-*i*Pr$_2$C$_6$H$_3$ (Dipp), X = Cl; Ar = 2,4,6-Me$_3$C$_6$H$_2$ (Mes) X = Cl, Br, I; **B**: R$^1$ = R$^2$ = SiMe$_3$; R$^1$ = H, R$^2$ = Dipp, 2,6-MesC$_6$H$_3$ (Dmp), 2,6-DippC$_6$H$_3$; **C**: R$^3$ = CH(SiMe$_3$)$_2$, Dmp; **D**: Ar′ = Dipp (**D1**), Mes (**D2**), R$^4$ = H; Ar′ = Dipp, R$^4$ = Me (**D3**), R$^4$ = C$_6$H$_4$-4-Et, Ar′ = Dipp (**D4**).

An attractive feature of RE-NHCs is that they are open to electronic manipulation through alterations at the backbone ring positions.[74-80] One particular approach is to incorporate heteroatom substituents as has been used in the design of diamidocarbenes (DACs), which contain C=O groups α to the N atoms.[81-83] While 6-Mes and the

diamidocarbene analogue 6-MesDAC are essentially isostructural, the electronic properties of the latter are altered significantly, with the carbene exhibiting enhanced π-acceptor capabilities.[84-87]

Herein, we compare and contrast the impact of the ring-expanded diaminocarbenes 6-Mes and 7-Mes with that of 6-MesDAC on the structural and electronic properties of CpNi(NHC) complexes using X-ray crystallography coupled with theory (TD-DFT). Further insights into the structure and unpaired spin density distributions in these paramagnetic complexes have been obtained using continuous wave (CW) electron paramagnetic resonance (EPR) and electron nuclear double resonance (ENDOR) spectroscopy.

## Experimental

All manipulations were performed under an atmosphere of dry argon using standard Schlenk line or glovebox techniques and employed dried and degassed solvents. NMR spectra were recorded on Bruker Avance 500 and 400 spectrometers at 25 °C and internally referenced to residual solvent resonances. UV/Vis spectra were recorded on a Varian Cary 50 spectrophotometer. Elemental analyses were determined by Elemental Microanalysis Ltd, Okehampton, Devon, UK. 6-Mes,[62] 7-Mes,[62] 6-MesDAC[88] and CpNi($PPh_3$)Br[89] were prepared according to literature procedures.

**CpNi(6-Mes)Br (1Br).** A benzene (3 mL) solution of 6-Mes (333 mg, 1.04 mmol, 1.05 eq) was added to a benzene (3 mL) solution of CpNi($PPh_3$)Br (489 mg, 0.990 mmol) and the mixture stirred at room temperature for 2 h. The solvent was removed in vacuum and the residue was washed with hexane (3 x 10 mL) and extracted

with toluene (20 mL). After filtration, the solution was concentrated to ca. 5 mL. A purple microcrystalline powder of **1Br** formed after adding hexane (15 mL) to the solution. The crystals were isolated and dried in vacuo. Yield 356 mg (69%). Single crystals suitable for X-ray diffraction were formed by diffusion of hexane into a concentrated toluene solution of the compound. $^{1}$H NMR (400 MHz, $C_6D_6$): δ 6.99 (s, 2H, *m*-CH), 6.81 (s, 2H, *m*-CH), 4.56 (s, 5H, Cp), 2.79 (s, 6H, *o*-CH), 2.72 (m, 2H, N*CH*$_2$CH$_2$), 2.61 (m, 2H, N*CH*$_2$CH$_2$), 2.19 (s, 6H, *p*-CH$_3$), 1.91 (s, 6H, *o*-CH$_3$), 1.64 (m, 1H, NCH$_2$*CH*$_2$), 1.14 (dt, $^{3}J_{HH}$ = 4.3 Hz, $^{1}J_{HH}$ = 13.3 Hz, 1H, NCH$_2$*CH*$_2$). $^{13}$C{$^{1}$H} NMR (100 MHz, $C_6D_6$): δ 203.0 (s, NCN), 145.2 (s, *i*-C), 138.1 (s, *o*-C), 137.6 (s, *o*-C), 135.0 (s, *p*-C), 131.1 (s, *m*-CH), 128.7 (s, *m*-CH), 93.8 (s, Cp), 47.0 (s, N*C*H$_2$CH$_2$), 21.1 (s, *o*-CH$_3$), 21.1 (s, *p*-CH$_3$), 21.0 (s, NCH$_2$*C*H$_2$), 18.3 (s, *o*-CH$_3$). Anal. Calcd. (%) for $C_{27}H_{33}BrN_2Ni \cdot 0.25C_7H_8$ (547.21): C 63.11, H 6.45, N 5.12. Found C 63.16, H 6.37, N 5.12;

**CpNi(6-Mes) (1).** $KC_8$ (97.4 mg, 0.720 mmol) was added in small portions at 238 K to a toluene (12 mL) solution of **1Br** (343 g, 0.655 mmol). The reaction mixture was warmed to room temperature and stirred for 28 h before being filtered. The filtrate was concentrated to ca. 5 mL and then stored at 243 K to yield X-ray quality, yellow crystals of **1**. Yield 127 mg (44%). $^{1}$H NMR (500 MHz, $C_6D_6$): δ 10.8 (br s), 9.3 (br s), 7.5 (br s), -14.7 (br s), -47.7 (br s). $\mu_{eff}$ ($C_6D_6$) = 1.8(1) $\mu_B$. UV/Vis ($Et_2O$, $\lambda_{max}$ /nm, ($\varepsilon_{max}$ /L·mol$^{-1}$·cm$^{-1}$)): 342 (10600), 368 (11000), 418 (9700). Anal. Calcd. (%) for $C_{27}H_{33}N_2Ni$ (444.27): C 73.00, H 7.49, N 6.31. Found C 72.57, H 7.18, N 6.26.

**CpNi(7-Mes)Br (2Br).** A toluene (20 mL) solution of 7-Mes (537 mg, 1.60 mmol) was added dropwise at 193 K to a toluene (30 mL) solution of CpNi($PPh_3$)Br

(761 mg, 1.54 mmol) and the mixture stirred at room temperature for 1.5 h. The solvent was removed in vacuum and the residue washed with hexane (3 x 20 mL). After extraction with toluene (40 mL), the filtrate was concentrated to ca. 15 mL. Violet crystals formed upon cooling to 257 K. The crystals were washed with pentane (10 mL) and dried under vacuum. Yield 420 mg (51%). Single crystals suitable for X-ray diffraction were isolated from toluene/hexane. $^{1}$H NMR (400 MHz, $C_6D_6$): δ 7.01 (s, 2H, *m*-CH), 6.81 (s, 2H, *m*-CH), 4.52 (s, 5H, Cp), 3.46 (m, 2H, N*CH*$_2$CH$_2$), 2.96 (m, 2H, N*CH*$_2$CH$_2$), 2.91 (s, 6H, *o*-$CH_3$), 2.19 (s, 6H, *p*-$CH_3$), 1.94 (s, 6H, *o*-$CH_3$), 1.88 (m, 2H, NCH$_2$*CH*$_2$), 1.15 (m, 2H, NCH$_2$*CH*$_2$). $^{13}$C{$^{1}$H} NMR (100 MHz, $C_6D_6$): δ 215.7 (s, NCN), 147.1 (s, *i*-C), 138.2 (s, *o*-C), 137.3 (s, *o*-C), 135.0 (s, *p*-C), 131.3 (s, *m*-CH), 128.9 (s, *m*-CH), 94.0 (s, Cp), 54.8 (s, N*C*H$_2$CH$_2$), 24.9 (s, NCH$_2$*C*H$_2$), 21.9 (s, *o*-$CH_3$), 21.0 (s, *p*-$CH_3$), 19.1 (s, *o*-Mes$CH_3$). Anal. Calcd (%) for $C_{28}H_{35}BrN_2Ni$ (538.20): C 62.49, H 6.56, N 5.21. Found C 63.24, H 6.40, N 5.25.

**CpNi(7-Mes) (2).** As for **1** but using $KC_8$ (113 mg, 0.836 mmol) and a toluene (15 mL) solution of **2Br** (409 mg, 0.760 mmol) with stirring for 18 h. After filtration, the filtrate was concentrated to ca. 1 mL and layered with hexane (1.5 mL) to afford yellow, X-ray quality crystals of **2** upon cooling to 238 K. Yield 156 mg (46%). $^{1}$H NMR (500 MHz, $C_6D_6$): δ 15.1 (br s), 12.0 (br s), 11.3 (br s), 4.9 (br s), -7.5 (br s), -52.4 (br s). $\mu_{eff}$ ($C_6D_6$) = 1.9(1) $\mu_B$. UV/Vis ($Et_2O$, $\lambda_{max}$ /nm, ($\varepsilon_{max}$ /L·mol$^{-1}$·cm$^{-1}$)): 377 (10100), 446 (7100). Anal. Calcd for $C_{28}H_{35}N_2Ni$ (458.30): C 73.38, H 7.70, N 6.11; Found C 72.61, H 7.31, N 5.80.

**CpNi(6-MesDAC)Br (3Br).** A benzene (30 mL) solution of 6-MesDAC (990 mg, 2.63 mmol) and CpNi($PPh_3$)Br (1.22 g, 2.48 mmol) was stirred at room temperature for 2

h before being reduced to dryness. The residue was washed with hexane (3 x 20 mL) and extracted into toluene (60 mL). After filtration, the filtrate was concentrated to ca. 30 mL and cooled to 243 K to yield dark brown microcrystals. Yield 913 mg (59%). Single crystals suitable for X-ray diffraction formed upon diffusion of hexane into a concentrated toluene solution of **3Br**. $^{1}$H NMR (400 MHz, $C_6D_6$): δ 6.92 (s, 2H, *m*-CH), 6.70 (s, 2H, *m*-CH), 4.53 (s, 5H, Cp), 2.76 (s, 6H, *o*-$CH_3$), 2.12 (s, 6H, *p*-$CH_3$), 1.76 (s, 6H, *o*-$CH_3$), 1.60 (s, 3H, C($CH_3$)$_2$), 1.41 (s, 3H, C($CH_3$)$_2$). $^{13}$C{$^{1}$H} NMR (100 MHz, $C_6D_6$): δ 237.9 (s, NCN), 168.7 (s, CO), 139.4 (s, *i*-C), 139.2 (s, *p*-C), 138.3 (s, *o*-C), 135.7 (s, *o*-C), 131.1 (s, *m*-CH), 129.1 (s, *m*-CH), 95.8 (s, Cp), 51.4 (s, *C*($CH_3$)$_2$), 28.5 (s, C(*C*$H_3$)$_2$), 21.0 (s, *p*-$CH_3$), 20.9 (s, *o*-$CH_3$), 18.9 (s, C(*C*$H_3$)$_2$), 18.8 (s, *o*-$CH_3$). Anal. Calcd for $C_{29}H_{33}BrN_2NiO_2$·0.2($C_7H_8$) (598.62): C 61.00, H 5.83, N 4.68; Found C 61.08, H 5.65, N 4.12.

**CpNi(6-MesDAC) (3).** As for **1**, but using $KC_8$ (47.2 mg, 0.349 mmol), a toluene (5 mL) solution of **3Br** (199 g, 0.317 mmol) and stirring at room temperature for 47 h. Dark green crystals of **3** formed after concentrating the filtrate to 3 mL and cooling to 243 K. Yield 73 mg (46%). X-ray quality crystals were obtained by cooling a concentrated toluene/*n*-hexane solution of the complex to 238 K. $^{1}$H NMR (500 MHz, $C_6D_6$): δ 15.5 (br s), 12.0 (br s), 1.3 (br s). $\mu_{eff}$ ($C_6D_6$) = 1.9(1) $\mu_B$. UV/Vis ($Et_2O$, $\lambda_{max}$ /nm, ($\varepsilon_{max}$ /L·mol$^{-1}$·cm$^{-1}$)): 313 (10300), 442 (31400), 592 (9300). Anal. Calcd for $C_{29}H_{33}N_2NiO_2$ (500.29): C 69.62, H 6.65, N 5.60. Found: C 69.74, H 6.52, N 5.60;

**X-ray crystallography.** Data for **1-3**, as well as **1Br-3Br** (ESI), were collected using an Agilent SuperNova diffractometer and Cu-Kα radiation at 150 K (Table 1). Convergence was relatively straightforward throughout and only points of note are

mentioned hereafter. The nickel center and cyclopentadienyl ring in **3** were seen to be disordered over 2 sites in a 58:42 ratio. Some ADP restraints were included in the final least-squares cycles for the fractional occupancy disordered carbon atoms. The structure of **3** was also investigated at 273 K (Figure S10). The rationale was to investigate whether or not the disorder had been frozen into the sample by flash cooling before the X-ray experiment. Additionally, it was deemed interesting to probe whether or not the disorder ratio might alter with temperature as a means of gaining further insight into the disorder type present given the CW X-band EPR spectral features (vide infra). The room temperature solid state structure was revealed to have the same phase as that observed for **3** at 150 K. In addition, the disorder ratio refined to 55:45 at 273 K indicating that, in this instance, a distinction between dynamic and static disorder cannot be made via X-ray crystallography. The asymmetric unit in **1Br** (Figure S7) was seen to contain four molecules of the nickel complex and two molecules of toluene. One of the solvent molecules was refined as being disordered over two proximate sites in a 60:40 ratio. ADP restraints were applied to fractional occupancy carbons to assist convergence. In addition to one molecule of the carbene complex, the asymmetric unit in **3Br** (Figure S9) was seen to contain one half of a molecule of toluene, disordered over two positions. The disordered moieties of solvent exhibited site-occupancies of 28% and 22%, respectively. As the rings in each component were close to being overlaid, they were each treated as rigid hexagons in the refinement and ADP restraints were also included in this region to assist convergence. The methyl carbons (C30 and C30A) were refined subject to being located 1.54 Å from the carbon atoms to which they are bonded, respectively. In addition,

the C34A···C30A, C30A···C33A, C30···C35 and C30···C33 distances were restrained to being similar.

Crystallographic data for compounds **1Br**, **1**, **2Br**, **2**, **3Br**, **3** and **3a** have been deposited with the Cambridge Crystallographic Data Center as supplementary publication CCDC 1487678-1487684. Copies of the data can be obtained free of charge on application to CCDC, 12 Union Road, Cambridge CB2 1EZ, UK [fax(+44) 1223 336033, e-mail: deposit@ccdc.cam.ac.uk].

**EPR/ENDOR spectroscopy.** Samples for EPR and ENDOR measurements were prepared under an $N_2$ atmosphere in a glovebox. A solution of each complex was prepared by dissolving ca. 4 mg of **1**-**3** in 200 μL of dry THF (in all cases, a small quantity of dry toluene was also added to improve the quality of the polycrystalline glass formed in frozen solution, and thereby enhance the quality of the EPR spectra). The solutions were transferred to an EPR tube, sealed in the glove box and then cooled to 77 K before rapid transfer to the pre-cooled EPR cavity. The X-band CW EPR measurements were performed on a Bruker EMX spectrometer utilizing an ER4119HS resonator, 100 kHz field modulation at 140 K. Additional X-band EPR measurements were performed at variable temperatures (from 6-140 K) on a Bruker Elexsys E500 spectrometer equipped with an Oxford Instruments liquid-helium cryostat and an ER4119HS resonator operating at 100 KHz. The Q-band EPR and ENDOR measurements were also recorded on a Bruker Elexsys E500 spectrometer using a Bruker ER5106 QT-E Q-band resonator operating at 12.5 kHz field modulation. The ENDOR spectra were obtained using 1 dB RF power from an ENI 3200L RF amplifier at 100 kHz

RF modulation depth and 0.5 mW microwave power. EPR simulations were performed using the Easyspin toolbox.[90]

## Results and Discussion

**Synthesis of CpNi(RE-NHC)Br.** Complexes **1Br**-**3Br** were synthesized according to Scheme 2 upon reaction of 6- and 7-Mes or 6-MesDAC with equimolar $CpNi(PPh_3)Br$ at or below room temperature. $^{1}H$ and $^{31}P\{^{1}H\}$ NMR spectroscopy indicated that the phosphine substitution by carbene occurred within 2 h. The resulting nickel(II) products proved to be highly soluble in benzene, toluene or THF, but effectively insoluble in hexane; they were isolated in moderate yields and characterized by $^{1}H$ and $^{13}C\{^{1}H\}$ NMR spectroscopy, elemental analysis, and single-crystal X-ray diffraction measurements (ESI). The data for **1-Br** and **2-Br** matched those reported very recently by Buchowicz and co-workers who described the synthesis of these same compounds via an alternative route involving the reaction of $Ni(DME)Br_2$, LiCp, and in-situ generated 6- or 7-Mes.[91] **3-Br** yielded no real surprises in terms of characterization; as expected for a DAC ligand, the Ni-carbene bond length (1.8715(18) Å) was shorter than in either **1-Br** (1.9082(19) Å) or **2-Br** (1.9010(18) Å), while the $^{13}C$ carbene resonance was shifted further downfield (δ 237.9 c.f. **1-Br**: δ 203.0; **2-Br**: δ 215.7).[85, 92]

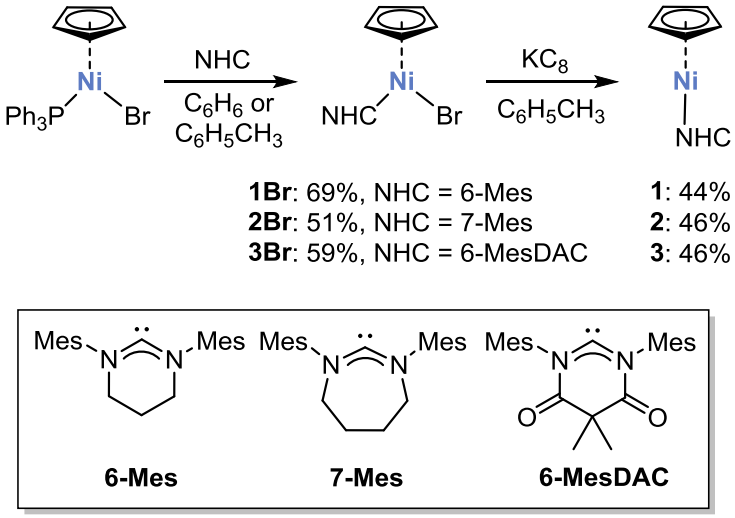


**Scheme 2.** Preparation of the nickel(II) halide precursors **1Br**-**3Br** and their reduction to the nickel(I) compounds **1**-**3**.

**Synthesis and Structural Identification of Ni(I) Complexes.** Reduction of **1Br**-**3Br** with $KC_8$ in toluene (Scheme 2) afforded the highly air-sensitive Ni(I) derivatives **1**-**3**, respectively, in yields of 44-46% upon low temperature crystallization. Single-crystal X-ray diffraction (Figure 1) in each case showed coordination of a nickel center by a carbene and an $\eta^5$-Cp ligand (analogous to **D**).[51-53] In this context, it is noteworthy that **3** features disorder of the CpNi fragment in a 58:42 ratio with respect to the DAC ligand (Figure 1, bottom). As for **D**, the geometries of the nickel centers with respect to the ligands in **1**-**3** is bent (Table 2), although the C(1)−Ni−$Cp_{centroid}$ angles (**1**: 159.1481(13)°); **2**: 160.565(3) Å; **3**: 161.1(3)/160.4(2) Å)[93] were significantly larger than in either CpNi(IPr) (**D1**, 154.3(1)°) or CpNi(IMes) (**D2**, 152.0(1)°), but smaller than in the $Cp^*$ derivative **D3** (164.8(1)°).[51-53] Moreover, whereas the Ni−$C_{ipso}$ distances to the flanking aryl rings in **D** were all greater than 3 Å (**D1**: 3.2438(11); **D2**: 3.40853(3); **D3**: 3.14599(4) Å) and therefore only slightly smaller than the sum of the van der Waals radii

for Ni and C (3.67 Å), the corresponding distances in **1**-**3** were considerably shorter (**1**: 2.7702(15) Å; **2**: 2.6056(15) Å; **3**: 2.666(2)/2.663(2) Å).[93] This most likely reflects the increased NCN angles of the RE-NHCs compared to their 5-membered counterparts.

The room temperature $^{1}$H NMR spectra of **1**-**3** in $C_6D_6$ exhibited broad, but diagnostic, signals in the range δ 15.5 to δ -52.4. The Cp ligands in **1** and **2** gave rise to significantly upfield resonances (δ -47.7, δ -52.4 respectively) similar to those observed in **D1** and **D2** (δ -40.7 and -38.2 respectively)[51-53] whereas, in the case of **3**, the resonances for both the Cp and 6-MesDAC appeared in the narrow range of δ 15.5 to δ 1.3.

**Table 2.** Selected bond lengths (Å) and angles (°) for **1**-**3**

| | **1** | **2** | **3**[a] |
|---|---|---|---|
| Ni(1)-C(1) | 1.8743(15) | 1.8759(15) | 1.8164(17) (1.8351(16)) |
| Ni(1)-$Cp_{centr.}$ | 1.7894(8) | 1.7951(8) | 1.792(4) (1.771(3)) |
| C(1)-Ni(1)-$Cp_{centr.}$ | 159.1 | 160.6 | 161.1 (160.4) |
| Ni(1)-C(1)-N(1) | 114.61(11) | 114.61(11) | 110.5(1) (133.7(1)) |
| Ni(1)-C(1)-N(2) | 128.67(11) | 128.67(11) | 134.1(1) (110.92(1)) |

[a] Metrics for the major and, in parentheses, minor components.

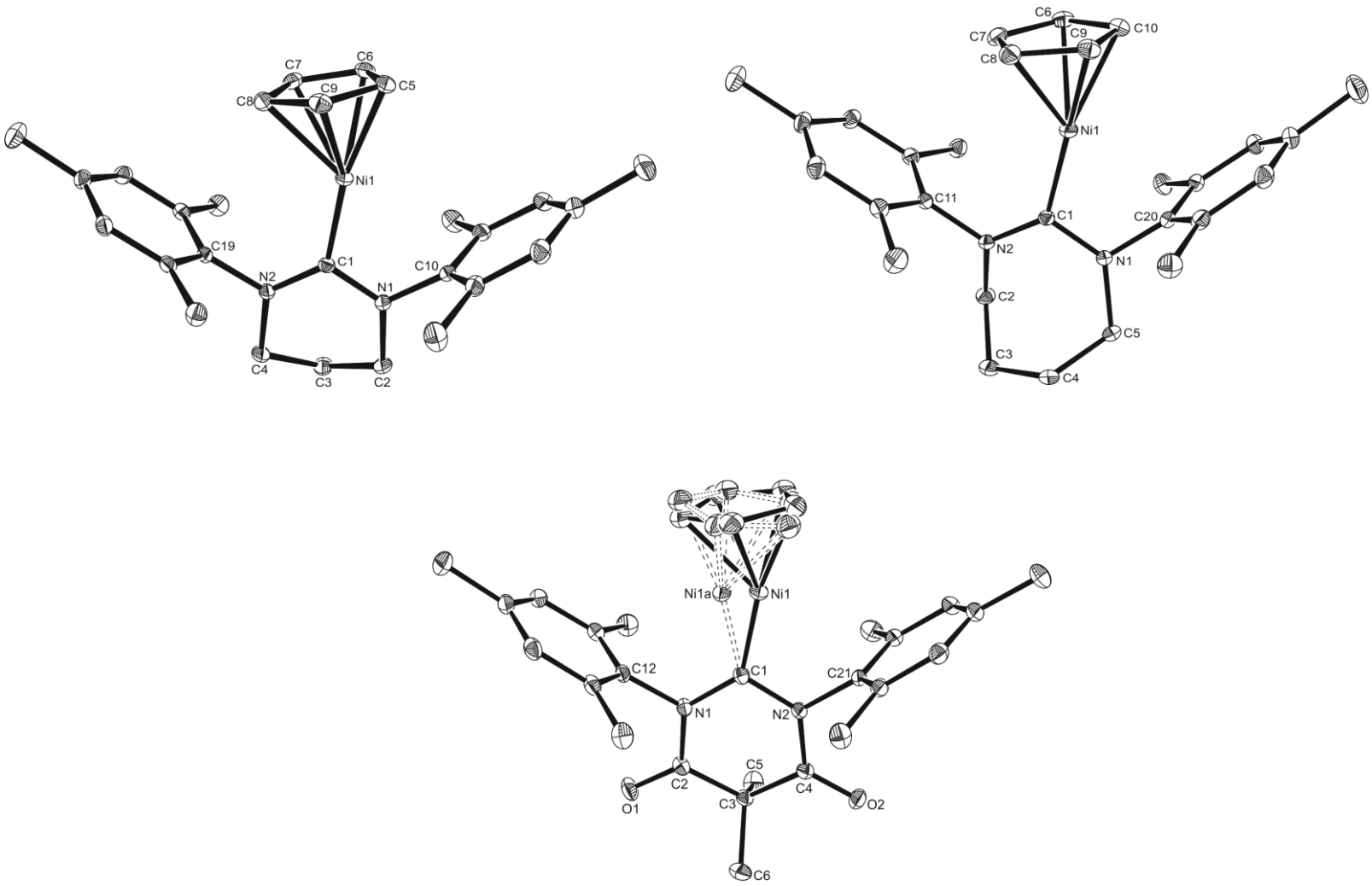


**Figure 1.** Molecular structures of (top left) CpNi(6-Mes) (**1**), (top right) CpNi(7-Mes) (**2**) and (bottom) CpNi(6-MesDAC) (**3**). Ellipsoids are shown at the 30% level. All hydrogen atoms have been removed for clarity.

**Electronic Properties of 1-3.** The solution magnetic moments (Evans method) were consistent with the presence of a single unpaired electron in **1**-**3**. The yellow-orange color of the diaminocarbene complexes was reflected in the appearance of intense absorption maxima at 342, 368, and 418 nm for **1**, and 377 and 446 nm for **2**. In contrast, dark green **3** showed bands at 313, 442, and 592 nm. To probe the electronic structure in more detail, (TD-)DFT calculations were performed (B3LYP/def2-TZVP level).[94-103] The optimized computed structures of **1**-**3** agreed well with the experimental structural data. According to a Löwdin population analysis, the spin density was located very strongly on the Ni center in all three compounds (**1**: 88%; **2**: 93%; **3**: 94%) and, as found in **D**, displayed a similar asymmetric shape directed slightly towards the *ipso*-C of an N-mesityl substituent. The calculations reproduced the experimental features of the UV-Vis spectra (ESI; Figures S11, S13 and S15). The calculated electronic transitions with the relevant molecular orbitals are given in the ESI (Tables S1-S3; Figures S12, S14 and S16). The results for complexes **1** and **2** indicate that for the visible bands at 368 and 418 nm (for **1**), as well as 377 and 446 nm (for **2**), the transitions have a complex composition. While the HOMOs feature partial metal and partial π-Cp character, the LUMO is mainly based on π*-orbitals of the mesityl substituents, with small contributions from the π*-orbitals of the carbene ligands. For compound **3**, similar contributing HOMOs are present with less metal character and an increased contribution of the π-orbitals of the mesityl moiety. In contrast to complexes **1** and **2**, the LUMOs of **3** feature significant contributions from the π*-orbitals of the DAC ligand (Figure S16), which might be due to the higher π-acceptor character.

**EPR and ENDOR Spectra of 1-3.** The continuous wave (CW) EPR and ENDOR spectra of the three paramagnetic Ni(I) compounds were recorded in frozen THF/toluene solution at X- (9.5 GHz) and Q- (34.5 GHz) band frequencies. The experimental and simulated EPR spectra for **1** are shown in Figure 2 (the corresponding EPR spectra for **2** and **3** are given in Figures S18 and S19). Owing to the well-defined rhombic nature of the **g** tensor, the EPR spectra were readily simulated using the Easyspin program[90] and the resulting spin Hamiltonian parameters are listed in Table 3. The pronounced $\Delta g$ shifts observed in the spectra are partially accounted for by the large spin-orbit coupling constant for Ni (565 $cm^{-1}$), whilst the low symmetry of the complexes themselves are responsible for the rhombic **g** tensor. The DFT derived *g* values calculated on the basis of the crystal structures are in reasonably good agreement with the experimental *g* values (Table 3). Although the overall magnitude of the experimental *g* values are larger than the DFT calculated values, the general trend observed in the $\Delta g$ shifts and decreasing $g_{iso}$ values for **1-3** match reasonably well (Table 3). In particular, the systematic decrease in all three $g_1$ values from **1** to **3** and the similarities in the $g_1$ values, are reproduced extremely well by the theoretical calculations. Whilst this trend is also reproduced in the calculated $g_2$ values for **1** and **2**, the theoretically predicted $g_2$ value for **3** is unexpectedly larger than the experimental value (Table 3) and we currently do not have an explanation for this observation. It is also interesting to note the unusual trend observed with respect to the *g*-strain in the complex, which causes the two low field *g* values to broaden more compared to the high field *g* value in the Q-band spectrum (Figure 2).

It should be stated that the *g* values of $d^9$ Ni(I) metal centers are highly dependent on the ligand coordination environment and many EPR studies of complexes bearing

Ni(I) centers that are 4-, 5- or 6-coordinate have been reported over the years,[104,105] with some recent studies focussing on the catalytic role of Ni(I).[106,107] By comparison, far fewer studies have been reported for low coordinate Ni(I) complexes.[71,108-114] One characteristic trend with the 3-coordinate systems, is that reversed *g* values are frequently observed compared to the higher coordinate systems, and the **g** tensor components are very dependent on whether the complex adopts a T- or Y-shape arrangement around the Ni(I) center.[109,110] This case of reversed EPR *g* values has been previously reported for the CpNi(I) complexes (Table 3).[51-53] The observed *g* values are consistent with the spin density plots for **1**-**3** which revealed considerable spin density localization on the nickel centers (Figure S17). It has also been reported by Hazari[53] that the SOMO and spin density plots for the analogous CpNi(IPr) complex had a significant Ni $d_{xz}$ orbital contribution. Assuming a similar orbital ground state in **1**-**3**, this would also account for the observed rhombic **g** tensor.

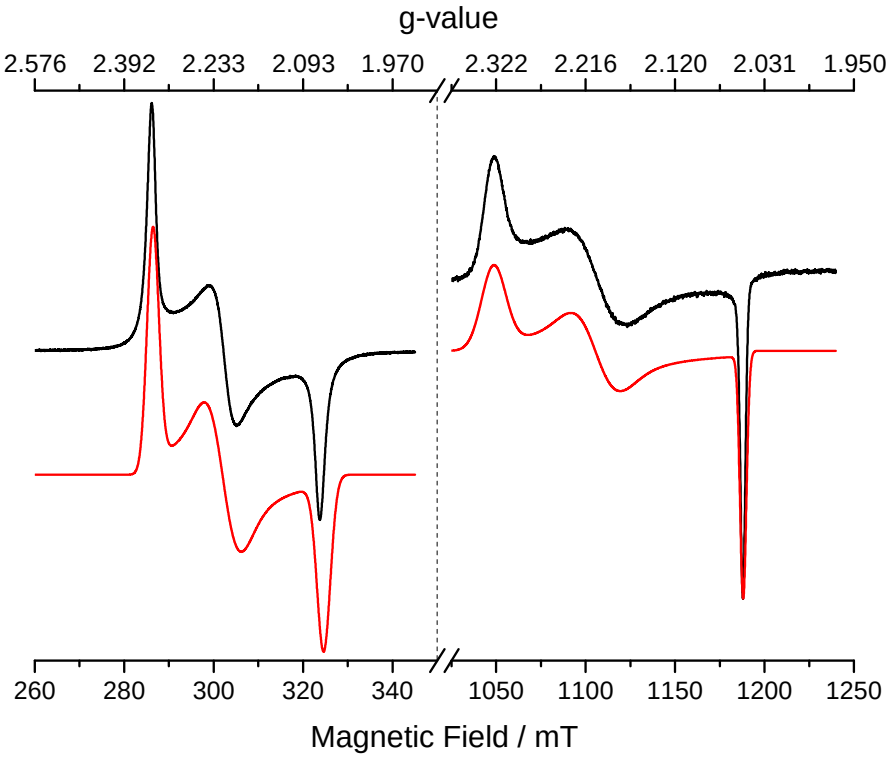


**Figure 2.** Experimental (black) and simulated (red) CW X- and Q-band EPR spectra of CpNi(6-Mes) (**1**) recorded at 140 K and 50 K respectively in frozen THF/toluene (95:5 v:v) solution. *Simulation parameters used in Easyspin:* **g** = [2.052, 2.204, 2.324]; linewidth simulated with **g** strain (labelled **gStrain** in Easyspin): **gStrain** (X-band) = [0.022, 0.055, 0.025]; **gStrain** (Q-band) = [0.007, 0.050, 0.035]. *Experimental conditions:* Microwave frequencies 9.320 GHz and 34.112 GHz; n# points, 4096.

The EPR *g* values for **1**-**3** are clearly very sensitive to changes in the NHC structure. Indeed, we have previously shown how the *g* values for the 3-coordinate Ni(I) complexes **E** shown in Scheme 1 varied markedly as a function of the NHC ring size.[71] Both Wolf[51,52] and Hazari[53] also reported variations in the *g* values of the Ni(I) complexes CpNi(NHC) with IPr ligands (Scheme 1, **D** and Table 3). Despite the almost

isostructural nature of **1** and **3**, the differences in the *g* values for both complexes (particularly evident in the $g_{iso}$ values) is very pronounced (Table 3), highlighting how the perturbations to the electronic structure of the Ni centers created by the DAC ligand can be manifested in the EPR spectra. Furthermore, the relative orientation of the **g** tensor with respect to the molecular axes and the spin density plot for complex **3** is shown in Figure 3. The **g** tensor orientation was determined based on the ORCA calculation of the **g** matrix using the crystal structure as the input file, with the $^{1}$H **A** matrix defined relative to the molecular frame. Although two components of *g* are clearly orthogonal to the Cp ring, one component is directed along the Cp-Ni-NHC direction, and this likely accounts for the sensitivity of the *g* values to changes in NHC structure.

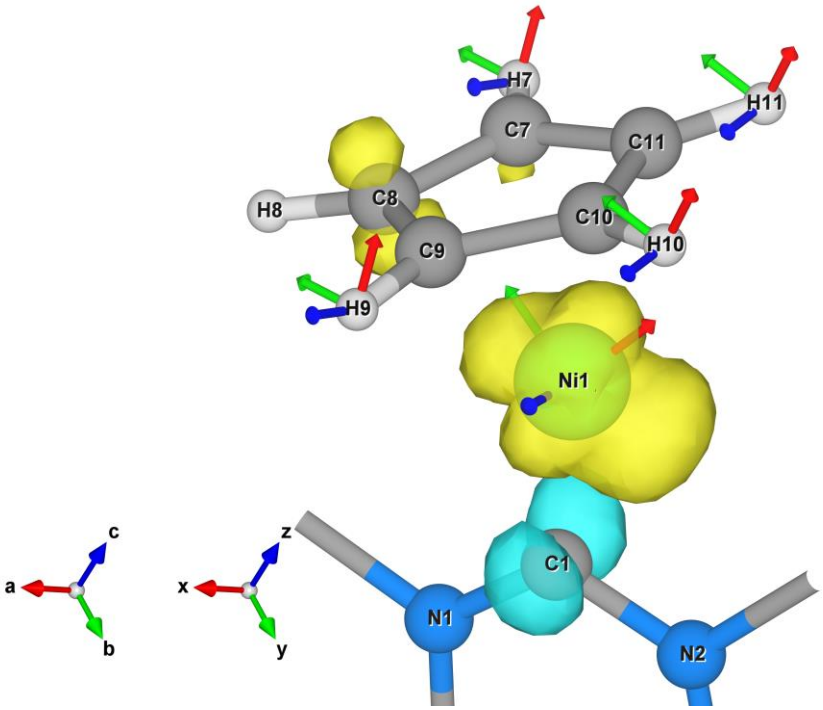

**Figure 3.** Orientations of the principal Ni **g** and Cp $^{H}$**A** tensors with respect to the molecular axes and spin density plot for complex **3**.

At 140 K, additional peaks were observed in the X-band CW EPR spectrum of **3** (Figure S19). Therefore, variable temperature EPR measurements were performed to examine the origin of these additional peaks. The resulting variable temperature X-band EPR spectra are shown in Figure 4 and clearly reveal a temperature dependent spectral profile. At temperatures below *ca*. 70 K, only a single Ni(I) center was detected (site Ni1 in Figure 1, characterized by the $g_{1,2,3}$ values of 2.032, 2.095, 2.262; Table 3), whereas above 70 K, the second Ni(I) center is simultaneously present (site Ni1a, with $g_{1,2,3}$ values of 2.054, 2.076, 2.262; Table 3). This second Ni(I) site appears to align with the observed disorder of the CpNi fragment over two similar positions, as detected in the X-ray structure (Figure 1). Indeed, the DFT calculated *g* values for this second Ni1a site, based on the coordinates from the X-ray crystal structure, are in very good agreement with the experimental values (Table 3).

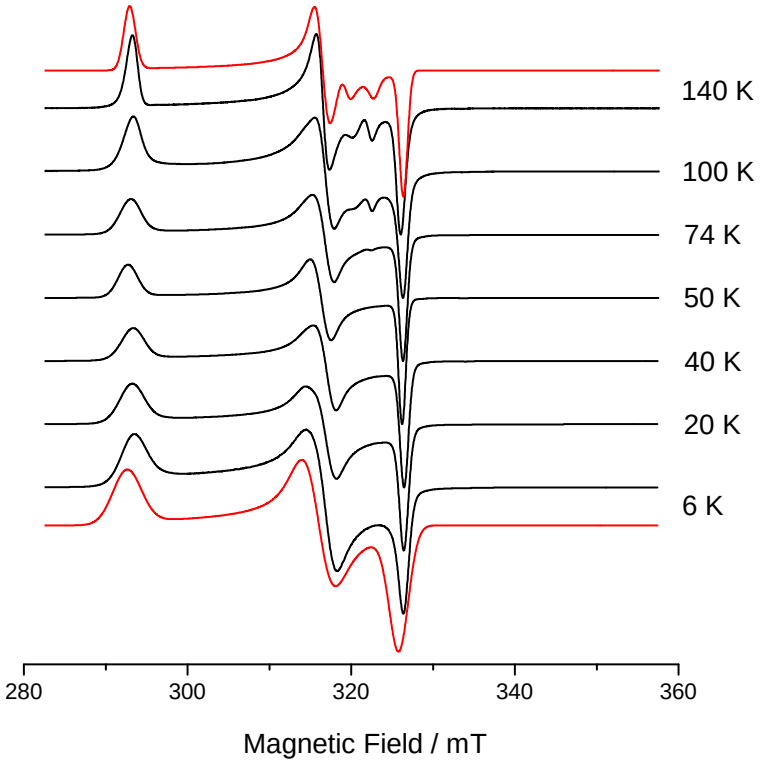


**Figure 4.** Experimental (black) and simulated (red) CW X-band EPR spectra of CpNi(6-MesDAC) (**3**) recorded at variable temperatures (6-140 K) in frozen THF/toluene (95:5 v:v) solution.

According to the EPR simulations, the relative abundances of the two sites Ni1:Ni1a at 140 K are *ca*. 90:10, whereas below 70 K only site Ni1 is observed (Figure 4). Although the crystal structures show a relatively consistent disorder ratio between Ni1 and Ni1a, which appears to be temperature independent, it must be borne in mind that crystallography cannot easily discriminate between static and dynamic disorder since the electron density maps represent averages of the molecular conformations for the whole crystal. The variable temperature EPR data (recorded in frozen solution, as opposed to the single crystal, where the relative populations may be expected to be different)

suggests that a dynamic process is certainly occurring such that the relative equilibrium populations between the two sites, visible on the EPR timescale, is strongly influenced by the temperature. Further analysis is required to understand the nature of the dynamic model responsible for the variable site occupancies detected by EPR for **3**.

Owing to the strong interaction between the Cp ring and the Ni(I) centers, angular selective Q-band $^{1}$H ENDOR experiments were also performed on **1**-**3** in order to measure the Cp $^{1}$H couplings. The resulting experimental and simulated spectra for **3** are shown in Figure 5 (the corresponding spectra for **1** and **2** are given in Figures S20 and S21). Although the overall profiles of the ENDOR spectra were relatively similar for all three complexes, the magnitude of the couplings generally appeared larger for **3** compared to **1** and **2** (Figure S22).

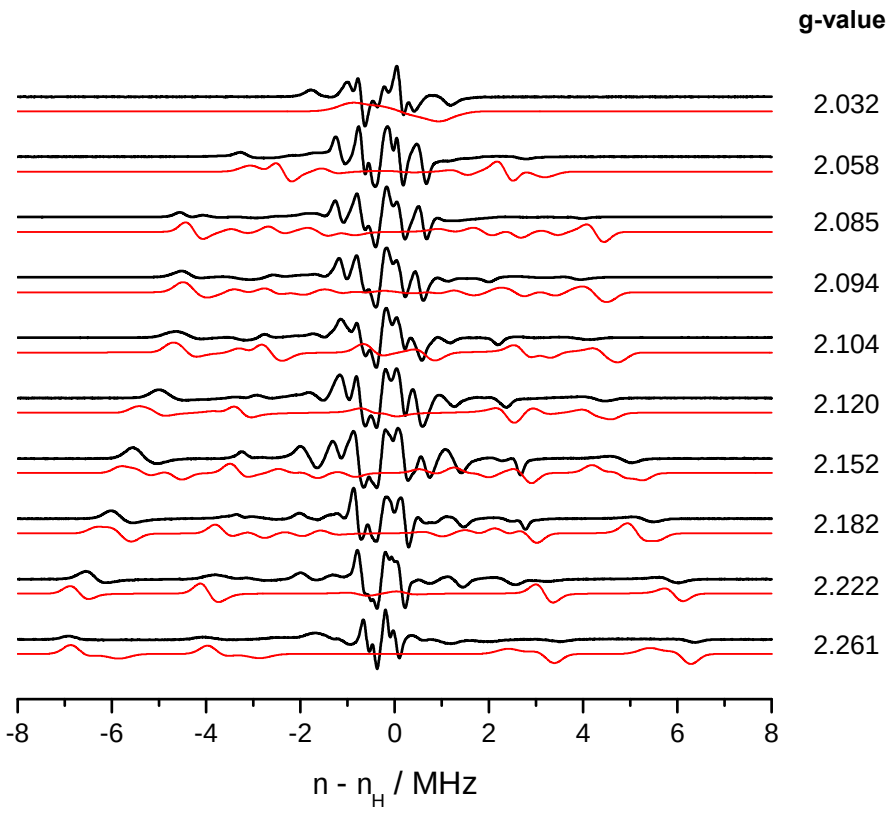

**Figure 5.** Experimental (black trace) and simulated (red trace) CW Q-band $^{1}$H ENDOR spectra of CpNi(6-MesDAC) (**3**) recorded in frozen THF solution (10 K). The *g* values corresponding to the static magnetic field positions used for the ENDOR measurement are given in the figure. The ENDOR spectra are plotted as the difference from the $^{1}$H Larmor frequency ($\nu_H \approx 15$ MHz). *Simulation parameters used in Easyspin:* **g**, **gFrame**, **A**, **AFrame** are reported in Tables 3 and 4, ENDOR linewidth, 0.40 MHz.

Due to the rhombic **g** tensor, the DFT calculated $^{1}$H tensors were used as a starting point for the ENDOR simulations, particularly in defining the Euler angles of the $^{H}$**A** tensor with respect to the molecular frame and **g** frame. According to the DFT calculations, the five Cp ring protons were all found to be inequivalent (Table 4), as expected for the bent orientation of the Cp ring with respect to the Ni-NHC orientation. Nevertheless, some of these Cp ring protons produce similar $^{1}$H hyperfine tensors (or at least within the resolution of the experimental powder ENDOR spectra, some of these tensors would appear indistinguishable).[115-118] The two Cp protons labelled $H^{10,11}$ (see Figure 3 for labels) produce the largest proton couplings (labelled $H(Cp)_{large}$ in Table 4), which are clearly observable in the ENDOR spectra, followed by a second set of protons which produce a relatively smaller coupling (labelled $H(Cp)_{small}$ in Table 4) arising from the two Cp protons labelled $H^{7,9}$. Only these two sets of proton couplings (referred to as $H(Cp)_{large}$ and $H(Cp)_{small}$), with $a_{iso}$ values of -6.3 and 3.23 MHz respectively, were included in the ENDOR simulations. For clarity, some of the experimental and deconvoluted $^{1}$H ENDOR simulations for CpNi(6-MesDAC) (**3**) at three selected field positions are shown in Figure 6. The remaining Cp proton (labelled $H^{8}$), with a calculated

$a_{iso}$ of only -0.1 MHz (Table S4) was not included in the simulation, as the peaks could not be identified in the experimental spectrum with a sufficiently high degree of accuracy. In addition, the peaks from this remaining Cp proton overlap with the weaker couplings (< 1 MHz) arising from the remote protons of the NHC ring (as determined by the ORCA calculations), and these latter, weak couplings were also not included in the simulation.

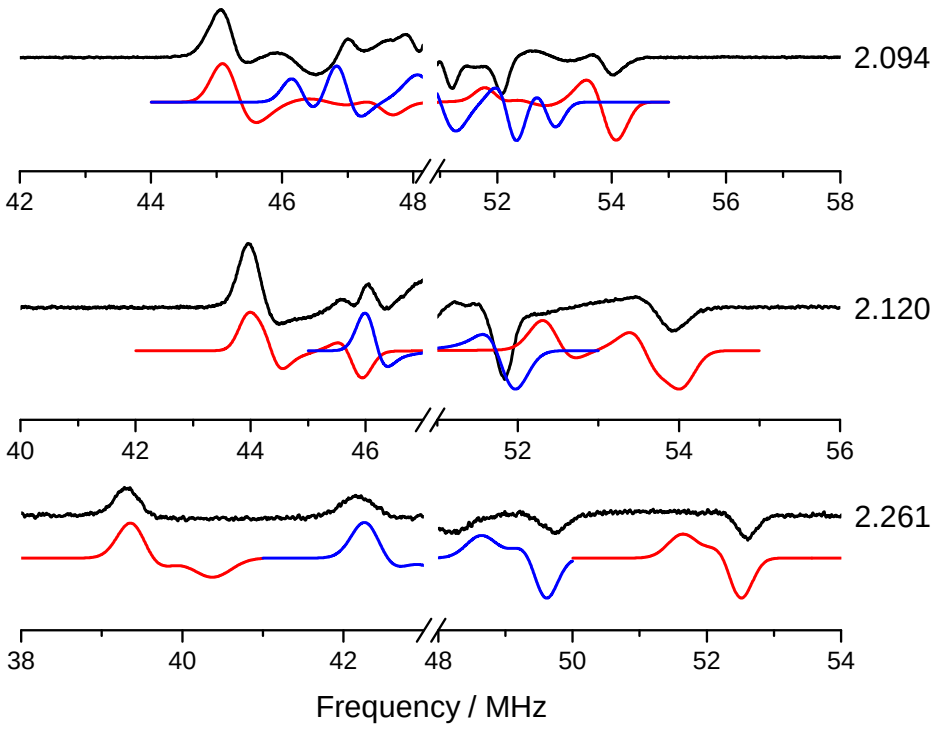


**Figure 6.** Experimental (black trace) and simulated CW Q-band $^{1}$H ENDOR spectra of CpNi(6-MesDAC) (**3**) recorded in frozen THF solution (10 K) at the three static field positions corresponding to the *g* values of 2.094, 2.120 and 2.261. The x-axis scale shows the absolute ENDOR frequencies. Red trace = simulation for H(Cp)$_{large}$ only, blue trace = simulation for H(Cp)$_{small}$ only (see Table 4 for parameters).

The experimental and simulated $^{1}$H ENDOR spectra for **1** and **2** are given in Figures S20 and S21, and the agreement between the experimental and simulated spectra is very good (Table 4). The principal components of the Cp $^{H}$**A** tensors for **1** and **2** were similar to each other (mirroring the similarities in the *g* values discussed earlier), compared to the slightly larger magnitude of the $^{H}$**A** tensors observed for **3**. With the exception of one proton, it should be noted that the Cp $^{1}$H hyperfine couplings in all three complexes are quite large, and this is largely due to the combination of the relatively short Ni-$^{1}$H(Cp) distances (these vary from 2.70 to 3.07 Å giving dipolar values from $A_{\|}$ = 8.0, $A_{\perp}$ = -4.0 MHz to $A_{\|}$ = 5.5, $A_{\perp}$ = -2.7 MHz in a classic point dipole approximation; Table S4) along with the appreciable Fermi contact contribution. Indeed, the $^{1}$H hyperfine couplings for $\eta^5$ coordinated Cp rings or $\eta^6$ coordinated arene rings in paramagnetic first row transition metal complexes are generally large, so the current findings are consistent with previous reports.[119-121] The contribution of the dominant anisotropic hyperfine terms coupled with the appreciable $a_{iso}$ terms for the Cp $^{1}$H's confirm the small amount of unpaired spin associated with the Cp ring, which is consistent with the calculated SOMOs of the complexes (Figure S17). It is interesting to note the slightly different nature of the SOMO in **3** compared to **1** and **2**, which also offers a potential explanation for the differences observed in the hyperfine values of **3** relative to **1** and **2**. Therefore the electronic perturbations to the CpNi(NHC) complex **3** created by the diamidocarbenes (DACs), is clearly manifested not only through differences in the UV spectra, differences in the SOMO and differences in the EPR *g* values, but also through subtle variations to the spin densities on the Cp ring protons as revealed by $^{1}$H ENDOR spectroscopy.

## Conclusions

Potassium graphite reduction of the Ni(II) ring-expanded N-heterocyclic diamino/diamidocarbene complexes CpNi(RE-NHC)Br produces the paramagnetic CpNi(RE-NHC) complexes (RE-NHC = 6-Mes (**1**), 7-Mes (**2**), 6-MesDAC (**3**). The structure of these three complexes was investigated by X-ray diffraction, DFT calculations, and EPR/ENDOR spectroscopy. The X-ray structures confirmed that the nickel centers in **1**-**3** are coordinated to the RE-NHC and the $\eta^5$-Cp ligand similar to the previously described 5-membered ring NHC complexes **D**.[51-53] In the case of the diamidocarbene complex **3**, the molecular structure revealed the CpNi fragment was disordered over two positions.

According to the DFT calculations, the spin densities in **1**-**3** were localized primarily on the Ni centers in all cases. The results obtained from the EPR/ENDOR measurements are consistent with the structures determined crystallographically. The rhombic **g** tensor displayed considerable anisotropy, as expected for low symmetry Ni(I) centers, with the smallest deviations from $g_e$ found in the diamidocarbene complex **3**, highlighting the electronic perturbation that results from the presence of the DAC ligand. Variable temperature EPR measurements of **3** also revealed the presence of a second Ni(I) center at temperatures above 70 K. The calculated *g* values for this second Ni(I) center are consistent with the nickel site (Ni1a) present in the minor disordered component present in the X-ray structure. A dynamic equilibrium between these two sites, which is manifested on the EPR timescale, appears to be responsible for the temperature dependent profile of the complex in frozen solution. The $^1$H hyperfine tensors for the Cp ring protons were also evaluated through simulation of the angular

selective ENDOR measurements. Whilst the structures of the tensors were similar for the three complexes, a slightly higher spin density was detected on the Cp ring for **3** compared to **1** and **2**.

It remains to be established whether the electronic differences we have seen translate into variations in reactivity. However, given the high levels of both stoichiometric and catalytic reactivity seen with the 5-membered ring NHC analogues[51-53] (**D** in Scheme 1), the recently reported catalytic C-C coupling activity of the corresponding Ni(II) precursors **1**-**Br** and **2**-**Br**[91] (shown herein to be readily accessible by straightforward phosphine exchange by a corresponding free RE-NHC in an easy and useful synthetic method) and the fact that variations of the substituents in RE-NHCs is known to have an impact in catalysis,[55,71] we are hopeful that studies to elucidate this will be forthcoming.

**Supporting Information Available:** $^{1}$H and $^{13}$C{$^{1}$H} NMR spectra for **1Br-3Br** and **1-3**, experimental UV-vis spectra, TD-DFT calculations and computational details, EPR spectra of **2-3**, $^{1}$H ENDOR spectra for **1-2**, point dipole calculation of the $^{1}$H Cp dipolar couplings, Cartesian coordinates for **1-3**. This material is available free of charge via the Internet at http://pubs.acs.org.

**Corresponding Authors**

*(D.M.M.) E-mail: MurphyDM@cardiff.ac.uk.

*(M.K.W) E-mail: M.K.Whittlesey@bath.ac.uk.

*(R.W.) E-mail: robert.wolf@ur.de.

Notes

The authors declare no competing financial interest.

**Acknowledgement.** We acknowledge the Deutsche Forschungsgemeinschaft and the German Academic Exchange Service (to SP) and EPSRC (EP/K017322/1 for AF) for financial support.

**References**

(1) Ragsdale, S. W.; Kumar, M. Nickel-Containing Carbon Monoxide Dehydrogenase/Acetyl-CoA Synthase. *Chem. Rev.* **1996**, *96*, 2515-2539.

(2) Finazzo, C.; Harmer, J.; Bauer, C.; Jaun, B.; Duin, E. C.; Mahlert, F.; Goenrich, M.; Thauer, R. K.; Van Doorslaer, S.; Schweiger, A. Coenzyme B Induced Coordination of Coenzyme M Via its Thiol Group to Ni(I) of F-430 in Active Methyl-Coenzyme M Reductase. *J. Am. Chem. Soc.* **2003**, *125*, 4988-4989.

(3) Ragsdale, S. W. Metals and their Scaffolds to Promote Difficult Enzymatic Reactions. *Chem. Rev.* **2006**, *106*, 3317-3337.

(4) Jeoung, J. H.; Dobbek, H. Carbon dioxide Activation at the Ni,Fe-Cluster of Anaerobic Carbon Monoxide Dehydrogenase. *Science* **2007**, *318*, 1461-1464.

(5) Yang, N.; Reiher, M.; Wang, M.; Harmer, J.; Duin, E. C. Formation of a Nickel-Methyl Species in Methyl-Coenzyme M Reductase, an Enzyme Catalyzing Methane Formation. *J. Am. Chem. Soc.* **2007**, *129*, 11028-11029.

(6) Evans, D. J. Chemistry Relating to the Nickel Enzymes CODH and ACS. *Coord. Chem. Rev.* **2005**, *249*, 1582-1595.

(7) Harmer, J.; Finazzo, C.; Piskorski, R.; Ebner, S.; Duin, E. C.; Goenrich, M.; Thauer, R. K.; Reiher, M.; Schweiger, A.; Hinderberger, D.; Jaun, B. A Nickel Hydride Complex in the Active Site of Methyl-Coenzyme M Reductase: Implications for the Catalytic Cycle. *J. Am. Chem. Soc.* **2008**, *130*, 10907-10920.

(8) Scheller, S.; Goenrich, M.; Boecher, R.; Thauer, R. K.; Jaun, B. The Key Nickel Enzyme of Methanogenesis Catalyses the Anaerobic Oxidation of Methane. *Nature* **2010**, *465*, 606-608.

(9) Scheller, S.; Goenrich, M.; Mayr, S.; Thauer, R. K.; Jaun, B. Intermediates in the Catalytic Cycle of Methyl Coenzyme M Reductase: Isotope Exchange is Consistent with Formation of a Sigma-Alkane-Nickel Complex. *Angew. Chem. Int. Ed.* **2010**, *49*, 8112-8115.

(10) Li, X. H.; Telser, J.; Kunz, R. C.; Hoffman, B. M.; Gerfen, G.; Ragsdale, S. W. Observation of Organometallic and Radical Intermediates Formed during the Reaction of Methyl-Coenzyme M Reductase with Bromoethanesulfonate. *Biochemistry* **2010**, *49*, 6866-6876.

(11) Can, M.; Armstrong, F. A.; Ragsdale, S. W. Structure, Function, and Mechanism of the Nickel Metalloenzymes, CO Dehydrogenase, and Acetyl-CoA Synthase. *Chem. Rev.* **2014**, *114*, 4149-4174.

(12) Wongnate, T.; Sliwa, D.; Ginovska, B.; Smith, D.; Wolf, M. W.; Lehnert, N.; Raugei, S.; Ragsdale, S. W. The Radical Mechanism of Biological Methane Synthesis by Methyl-Coenzyme M Reductase. *Science* **2016**, *352*, 953-958.

(13) Tsou, T. T.; Kochi, J. K. Mechanism of Biaryl Synthesis with Nickel-Complexes. *J. Am. Chem. Soc.* **1979**, *101*, 7547-7560.

(14) Tsou, T. T.; Kochi, J. K. Nickel Catalysis in Halogen Exchange with Aryl and Vinylic Halides. *J. Org. Chem.* **1980**, *45*, 1930-1937.

(15) Mindiola, D. J.; Hillhouse, G. L. Terminal Amido and Imido Complexes of Three-Coordinate Nickel. *J. Am. Chem. Soc.* **2001,** *123*, 4623-4624.

(16) Hu, X. L.; Castro-Rodriguez, I.; Meyer, K. Synthesis and Characterization of Electron-Rich Nickel Tris-Carbene Complexes. *Chem. Commun.* **2004**, 2164-2165.

(17) Melenkivitz, R.; Mindiola, D. J.; Hillhouse, G. L. Monomeric Phosphido and Phosphinidene Complexes of Nickel. *J. Am. Chem. Soc.* **2002**, *124*, 3846-3847.

(18) Ito, M.; Matsumoto, T.; Tatsumi, K. Synthesis and Reactions of Mono- and Dinuclear Ni(I) Thiolate Complexes. *Inorg. Chem.* **2009**, *48*, 2215-2223.

(19) Jones, C.; Schulten, C.; Fohlmeister, L.; Stasch, A.; Murray, K. S.; Moubaraki, B.; Kohl, S.; Ertem, M. Z.; Gagliardi, L.; Cramer, C. J. Bulky Guanidinato Nickel (I) Complexes: Synthesis, Characterization, Isomerization, and Reactivity Studies. *Chem. Eur. J.* **2011**, *17*, 1294-1303.

(20) Beck, R.; Johnson, S. A. Dinuclear Ni(I)-Ni(I) Complexes with Syn-Facial Bridging Ligands from Ni(I) Precursors or Ni(II)/Ni(0) Comproportionation. *Organometallics* **2013**, *32*, 2944-2951.

(21) Faust, M.; Bryan, A. M.; Mansikkamaki, A.; Vasko, P.; Olmstead, M. M.; Tuononen, H. M.; Grandjean, F.; Long, G. J.; Power, P. P. The Instability of $Ni\{N(SiMe_3)_2\}_2$: A Fifty Year Old Transition Metal Silylamide Mystery. *Angew. Chem. Int. Ed.* **2015**, *54*, 12914-12917.

(22) Chakraborty, U.; Mühldorf, B.; van Velzen, N. J. C.; de Bruin, B.; Harder, S.; Wolf, R. [$Cp^{Ar}$Ni{Ga(nacnac)}]: An Open-Shell Nickel(I) Complex Supported by a Gallium(I) Carbenoid ($Cp^{Ar}$ = $C_5(C_6H_4$-4-Et$)_5$, nacnac = HC[C(Me)N($C_6H_3$)-2,6-$^{i}Pr_2]_2$). *Inorg. Chem.* **2016**, *55*, 3075-3078.

(23) Anderson, T. J.; Jones, G. D.; Vicic, D. A. Evidence for a Ni(I) Active Species in the Catalytic Cross-Coupling of Alkyl Electrophiles. *J. Am. Chem. Soc.* **2004**, *126*, 8100-8101.

(24) Weng, Z. Q.; Teo, S.; Koh, L. L.; Hor, T. S. A. Ethylene Oligomerization at Coordinatively and Electronically Unsaturated Low-Valent Nickel. *Angew. Chem. Int. Ed.* **2005**, *44*, 7560-7564.

(25) Wang, H. Y.; Meng, X.; Jin, G. X. Synthesis, Molecular Structure and Norbornene Polymerization Behavior of Three-Coordinate Nickel(I) Complexes with Chelating Anilido-Imine Ligands. *Dalton Trans.* **2006**, 2579-2585.

(26) Vogt, M.; de Bruin, B.; Berke, H.; Trincado, M.; Grützmacher, H. Amino Olefin Nickel(I) and Nickel(0) Complexes as Dehydrogenation Catalysts for Amine Boranes. *Chem. Sci.* **2011**, *2*, 723-727.

(27) Lipschutz, M. I.; Tilley, T. D. Carbon-Carbon Cross-Coupling Reactions Catalyzed by a Two-Coordinate Nickel(II)-Bis(amido) Complex via Observable $Ni^{I}$, $Ni^{II}$, and $Ni^{III}$ Intermediates. *Angew. Chem. Int. Ed.* **2014**, *53*, 7290-7294.

(28) Vedernikov, A. N. Mechanism of the Kumada-Corriu Cross-Coupling Catalyzed by Low-Coordinate Bis(amido)-Nickel Complexes: Identification of Nickel(I)-(III) Catalytic Intermediates. *ChemCatChem* **2014**, *6*, 2490-2492.

(29) Guard, L. M.; Beromi, M. M.; Brudvig, G. W.; Hazari, N.; Vinyard, D. J. Comparison of dppf-Supported Nickel Precatalysts for the Suzuki-Miyaura Reaction: The Observation and Activity of Nickel(I). *Angew. Chem. Int. Ed.* **2015**, *54*, 13352-13356.

(30) Kieber-Emmons, M. T.; Schenker, R.; Yap, G. P. A.; Brunold, T. C.; Riordan, C. G. Spectroscopic Elucidation of a Peroxo $Ni_2(\mu\text{-}O_2)$ Intermediate Derived from a Nickel(I) Complex and Dioxygen. *Angew. Chem. Int. Ed.* **2004**, *43*, 6716-6718.

(31) Kieber-Emmons, M. T.; Riordan, C. G. Dioxygen Activation at Monovalent Nickel. *Acc. Chem. Res.* **2007**, *40*, 618-625.

(32) Adhikari, D.; Mossin, S.; Basuli, F.; Dible, B. R.; Chipara, M.; Fan, H.; Huffman, J. C.; Meyer, K.; Mindiola, D. J. A Dinuclear Ni(I) System Having a Diradical $Ni_2N_2$ Diamond Core Resting State: Synthetic, Structural, Spectroscopic Elucidation, and Reductive Bond Splitting Reactions. *Inorg. Chem.* **2008**, *47*, 10479-10490.

(33) Fullmer, B. C.; Fan, H. J.; Pink, M.; Caulton, K. G. O/C bond cleavage of $CO_2$ by Ni(I). *Inorg. Chem.* **2008**, *47*, 1865-1867.

(34) Yao, S. L.; Xiong, Y.; Milsmann, C.; Bill, E.; Pfirrmann, S.; Limberg, C.; Driess, M. Reversible $P_4$ Activation with Nickel(I) and an $\eta^3$-Coordinated Tetraphosphorus Ligand between Two Ni(I) Centers. *Chem. Eur. J.* **2010**, *16*, 436-439.

(35) Horn, B.; Pfirrmann, S.; Limberg, C.; Herwig, C.; Braun, B.; Mebs, S.; Metzinger, R. $N_2$ Activation in $Ni^I$-NN-$Ni^I$ Units: The Influence of Alkali Metal Cations and CO Reactivity. *Z. Anorg. Allg. Chem.* **2011**, *637*, 1169-1174.

(36) Iluc, V. M.; Hillhouse, G. L. Arrested 1,2-Hydrogen Migration from Silicon to Nickel upon Oxidation of a Three-Coordinate Ni(I) Silyl Complex. *J. Am. Chem. Soc.* **2010**, *132*, 11890-11892.

(37) Iluc, V. M.; Hillhouse, G. L. Hydrogen-Atom Abstraction from Ni(I) Phosphido and Amido Complexes Gives Phosphinidene and Imide Ligands. *J. Am. Chem. Soc.* **2010**, *132*, 15148-15150.

(38) Yao, S. L.; Driess, M. Lessons from Isolable Nickel(I) Precursor Complexes for Small Molecule Activation. *Acc. Chem. Res.* **2012**, *45*, 276-287.

(39) Beck, R.; Shoshani, M.; Krasinkiewicz, J.; Hatnean, J. A.; Johnson, S. A. Synthesis and Chemistry of Bis(triisopropylphosphine) Nickel(I) and Nickel(0) Precursors. *Dalton Trans.* **2013**, *42*, 1461-1475.

(40) Horn, B.; Limberg, C.; Herwig, C.; Braun, B. Nickel(I)-Mediated Transformations of Carbon Dioxide in Closed Synthetic Cycles: Reductive Cleavage and Coupling of $CO_2$ Generating $Ni^{I}CO$, $Ni^{II}CO_3$ and $Ni^{II}C_2O_4Ni^{II}$ Entities. *Chem. Commun.* **2013**, *49*, 10923-10925.

(41) Lipschutz, M. I.; Yang, X. Z.; Chatterjee, R.; Tilley, T. D. A Structurally Rigid Bis(amido) Ligand Framework in Low-Coordinate Ni(I), Ni(II), and Ni(III) Analogues Provides Access to a Ni(III) Methyl Complex via Oxidative Addition. *J. Am. Chem. Soc.* **2013**, *135*, 15298-15301.

(42) Schwab, M. M.; Himmel, D.; Kacprzak, S.; Kratzert, D.; Radtke, V.; Weis, P.; Ray, K.; Scheidt, E.-W.; Scherer, W.; de Bruin, B.; Weber, S.; Krossing, I. $[Ni(cod)_2][Al(OR^F)_4]$, A Source for Naked Nickel(I) Chemistry. *Angew. Chem. Int. Ed.* **2015**, *54*, 14706-14709.

(43) Miyazaki, S.; Koga, Y.; Matsumoto, T.; Matsubara, K. A New Aspect of Nickel-Catalyzed Grignard Cross-Coupling Reactions: Selective Synthesis, Structure, and Catalytic Behavior of a T-Shape Three-Coordinate Nickel(I) Chloride Bearing a Bulky NHC Ligand. *Chem. Commun.* **2010**, *46*, 1932-1934.

(44) Zhing, K. N.; Conda-Sheridan, M.; Cooke, S. R.; Louie, J. N-Heterocyclic Carbene Bound Nickel(I) Complexes and Their Roles in Catalysis. *Organometallics* **2011**, *30*, 2546-2552.

(45) Nagao, S.; Matsumoto, T.; Koga, Y.; Matsubara, K. Monovalent Nickel Complex Bearing a Bulky N-Heterocyclic Carbene Catalyzes Buchwald-Hartwig Amination of Aryl Halides under Mild Conditions. *Chem. Lett.* **2011**, *40*, 1036-1038.

(46) Laskowski, C. A.; Hillhouse, G. L. Two-Coordinate $d^9$ Complexes. Synthesis and Oxidation of NHC Nickel(I) Amides. *J. Am. Chem. Soc.* **2008**, *130*, 13846-13847.

(47) Laskowski, C. A.; Miller, A. J. M.; Hillhouse, G. L.; Cundari, T. R. A Two-Coordinate Nickel Imido Complex That Effects C-H Amination. *J. Am. Chem. Soc.* **2011**, *133*, 771-773.

(48) Laskowski, C. A.; Morello, G. R.; Saouma, C. T.; Cundari, T. R.; Hillhouse, G. L. Single-Electron Oxidation of N-Heterocyclic Carbene-Supported Nickel Amides Yielding Benzylic C-H Activation. *Chem. Sci.* **2013**, *4*, 170-174.

(49) Laskowski, C. A.; Bungum, D. J.; Baldwin, S. M.; Del Ciello, S. A.; Iluc, V. M.; Hillhouse, G. L. Synthesis and Reactivity of Two-Coordinate Ni(I) Alkyl and Aryl Complexes. *J. Am. Chem. Soc.* **2013**, *135*, 18272-18275.

(50) Lipschutz, M. I.; Tilley, T. D. Useful Method for the Preparation of Low-Coordinate Nickel(I) Complexes via Transformations of the Ni(I) Bis(amido) Complex K{Ni[N($SiMe_3$)(2,6-$^{i}Pr_2$-$C_6H_3$)]$_2$}. *Organometallics* **2014**, *33*, 5566-5570.

(51) Pelties, S.; Herrmann, D.; de Bruin, B.; Hartl, F.; Wolf, R. Selective $P_4$ Activation by an Organometallic Nickel(I) Radical: Formation of a Dinuclear Nickel(II) Tetraphosphide and Related Di- and Trichalcogenides. *Chem. Commun.* **2014**, *50*, 7014-7016.

(52) Chakraborty, U.; Urban, F.; Muhldorft, B.; Rebreyend, C.; de Bruin, B.; van Velzen, N.; Harder, S.; Wolf, R. Accessing the $Cp^{Ar}$Ni(I) Synthon: Reactions with N-Heterocyclic Carbenes, TEMPO, Sulfur, and Selenium. *Organometallics* **2016**, *35*, 1624-1631.

(53) Wu, J. G.; Nova, A.; Balcells, D.; Brudvig, G. W.; Dai, W.; Guard, L. M.; Hazari, N.; Lin, P. H.; Pokhrel, R.; Takase, M. K. Nickel(I) Monomers and Dimers with Cyclopentadienyl and Indenyl Ligands. *Chem. Eur. J.* **2014**, *20*, 5327-5337.

(54) Prakasham, A. P.; Ghosh, P. Nickel N-Heterocyclic Carbene Complexes and Their Utility in Homogeneous Catalysis. *Inorg. Chim. Acta* **2015**, *431*, 61-100.

(55) Henrion, M.; Ritleng, V.; Chetcuti, M. J. Nickel N-Heterocyclic Carbene-Catalyzed C-C Bond Formation: Reactions and Mechanistic Aspects. *ACS Catal.* **2015**, *5*, 1283-1302.

(56) Ritleng, V.; Henrion, M.; Chetcuti, M. J. Nickel N-Heterocyclic Carbene-Catalyzed C-Heteroatom Bond Formation, Reduction, and Oxidation: Reactions and Mechanistic Aspects. *ACS Catal.* **2016**, *6*, 890-906.

(57) Liu, C.; Tang, S.; Liu, D.; Yuan, J. W.; Zheng, L. W.; Meng, L. K.; Lei, A. W., Nickel-Catalyzed Heck-Type Alkenylation of Secondary and Tertiary α-Carbonyl Alkyl Bromides. *Angew. Chem. Int. Ed.* **2012**, *51*, 3638-3641.

(58) Li, Z.; Jiang, Y. Y.; Fu, Y. Theoretical Study on the Mechanism of Ni-Catalyzed Alkyl-Alkyl Suzuki Cross-Coupling. *Chem. Eur. J.* **2012**, *18*, 4345-4357.

(59) Sayyed, F. B.; Tsuji, Y.; Sakaki, S. The Crucial Role of a Ni(I) Intermediate in Ni-Catalyzed Carboxylation of Aryl Chloride with $CO_2$: A Theoretical Study. *Chem. Commun.* **2013**, *49*, 10715-10717.

(60) Cornella, J.; Gómez-Bengoa, E.; Martin, R. Combined Experimental and Theoretical Study on the Reductive Cleavage of Inert C-O Bonds with Silanes: Ruling out a Classical Ni(0)/Ni(II) Catalytic Couple and Evidence for Ni(I) Intermediates. *J. Am. Chem. Soc.* **2013**, *135*, 1997-2009.

(61) Wiese, S.; Aguila, M. J. B.; Kogut, E.; Warren, T. H. β-Diketiminato Nickel Imides in Catalytic Nitrene Transfer to Isocyanides. *Organometallics* **2013**, *32*, 2300-2308.

(62) Iglesias, M.; Beetstra, D. J.; Knight, J. C.; Ooi, L. L.; Stasch, A.; Coles, S.; Male, L.; Hursthouse, M. B.; Cavell, K. J.; Dervisi, A.; Fallis, I. A. Novel Expanded Ring N-Heterocyclic Carbenes: Free Carbenes, Silver Complexes, and Structures. *Organometallics* **2008**, *27*, 3279-3289.

(63) Kolychev, E. L.; Portnyagin, I. A.; Shuntikov, V. V.; Khrustalev, V. N.; Nechaev, M. S. Six- and Seven-Membered Ring Carbenes: Rational Synthesis of Amidinium Salts, Generation of Carbenes, Synthesis of Ag(I) and Cu(I) complexes. *J. Organomet. Chem.* **2009**, *694*, 2454-2462.

(64) Lu, W. Y.; Cavell, K. J.; Wixey, J. S.; Kariuki, B. First Examples of Structurally Imposing Eight-Membered-Ring (Diazocanylidene) N-Heterocyclic Carbenes: Salts, Free Carbenes, and Metal Complexes. *Organometallics* **2011**, *30*, 5649-5655.

(65) Dunsford, J. J.; Cavell, K. J.; Kariuki, B. M. Gold(I) Complexes Bearing Sterically Imposing, Saturated Six- and Seven-Membered Expanded Ring N-Heterocyclic Carbene Ligands. *Organometallics* **2012**, *31*, 4118-4121.

(66) Li, J.; Shen, W. X.; Li, X. R. Recent Developments of Expanded Ring N-Heterocyclic Carbenes. *Curr. Org. Chem.* **2012**, *16*, 2879-2891.

(67) Bramananthan, N.; Carmona, M.; Lowe, J. P.; Mahon, M. F.; Poulten, R. C.; Whittlesey, M. K. Rh-FHF and Rh-F Complexes Containing Small N-Alkyl Substituted Six-Membered Ring N-Heterocyclic Carbenes. *Organometallics* **2014**, *33*, 1986-1995.

(68) Phillips, N.; Dodson, T.; Tirfoin, R.; Bates, J. I.; Aldridge, S. Expanded-Ring N-Heterocyclic Carbenes for the Stabilization of Highly Electrophilic Gold(I) Cations. *Chem. Eur. J.* **2014**, *20*, 16721-16731.

(69) Jordan, A. J.; Wyss, C. M.; Bacsa, J.; Sadighi, J. P. Synthesis and Reactivity of New Copper(I) Hydride Dimers. *Organometallics* **2016**, *35*, 613-616.

(70) Davies, C. J. E.; Page, M. J.; Ellul, C. E.; Mahon, M. F.; Whittlesey, M. K. Ni(I) and Ni(II) Ring-Expanded N-Heterocyclic Carbene Complexes: C-H Activation, Indole Elimination and Catalytic Hydrodehalogenation. *Chem. Commun.* **2010**, *46*, 5151-5153.

(71) Page, M. J.; Lu, W. Y.; Poulten, R. C.; Carter, E.; Algarra, A. G.; Kariuki, B. M.; Macgregor, S. A.; Mahon, M. F.; Cavell, K. J.; Murphy, D. M.; Whittlesey, M. K. Three-Coordinate Nickel(I) Complexes Stabilised by Six-, Seven- and Eight-Membered Ring N-Heterocyclic Carbenes: Synthesis, EPR/DFT Studies and Catalytic Activity. *Chem. Eur. J.* **2013**, *19*, 2158-2167.

(72) Poulten, R. C.; López, I.; Llobet, A.; Mahon, M. F.; Whittlesey, M. K. Stereoelectronic Effects in C-H Bond Oxidation Reactions of Ni(I) N-Heterocyclic Carbene Complexes. *Inorg. Chem.* **2014**, *53*, 7160-7169.

(73) Poulten, R. C.; Page, M. J.; Algarra, A. G.; Le Roy, J. J.; López, I.; Carter, E.; Llobet, A.; Macgregor, S. A.; Mahon, M. F.; Murphy, D. M.; Murugesu, M.; Whittlesey, M. K. Synthesis, Electronic Structure, and Magnetism of $[Ni(6\text{-}Mes)_2]^+$: A Two-Coordinate Nickel(I) Complex Stabilized by Bulky N-Heterocyclic Carbenes. *J. Am. Chem. Soc.* **2013**, *135*, 13640-13643.

(74) Bazinet, P.; Yap, G. P. A.; Richeson, D. S. Constructing a Stable Carbene with a Novel Topology and Electronic Framework. *J. Am. Chem. Soc.* **2003**, *125*, 13314-13315.

(75) Scarborough, C. C.; Grady, M. J. W.; Guzei, I. A.; Gandhi, B. A.; Bunel, E. E.; Stahl, S. S. $Pd^{II}$ Complexes Possessing a Seven-Membered N-Heterocyclic Carbene Ligand. *Angew. Chem. Int. Ed.* **2005,** *44*, 5269-5272.

(76) Bazinet, P.; Ong, T. G.; O'Brien, J. S.; Lavoie, N.; Bell, E.; Yap, G. P. A.; Korobkov, I.; Richeson, D. S. Design of Sterically Demanding, Electron-Rich Carbene Ligands with the Perimidine Scaffold. *Organometallics* **2007**, *26*, 2885-2895.

(77) Siemeling, U.; Färber, C.; Leibold, M.; Bruhn, C.; Mücke, P.; Winter, R. F.; Sarkar, B.; von Hopffgarten, M.; Frenking, G.. Six-Membered N-Heterocyclic Carbenes with a 1,1'-Ferrocenediyl Backbone: Bulky Ligands with Strong Electron-Donor Capacity and Unusual Non-Innocent Character. *Eur. J. Inorg. Chem.* **2009**, 4607-4612.

(78) Iglesias, M.; Beetstra, D. J.; Cavell, K. J.; Deryisi, A.; Fallis, I. A.; Kariuki, B.; Harrington, R. W.; Clegg, W.; Horton, P. N.; Coles, S. J.; Hursthouse, M. B., Expanded-Ring and Backbone-Functionalised N-Heterocyclic Carbenes. *Eur. J. Inorg. Chem.* **2010**, 1604-1607.

(79) Newman, P. D.; Cavell, K. J.; Kariuki, B. M. Metal Complexes of Chiral NHCs Containing a Fused Six- and Seven-Membered Central Ring. *Organometallics* **2010**, *29*, 2724-2734.

(80) Siemeling, U.; Färber, C.; Bruhn, C.; Fürmeier, S.; Schulz, T.; Kurlemann, M.; Tripp, S. Group 10 Metal Complexes of a Ferrocene-Based N-Heterocyclic Carbene: Syntheses, Structures and Catalytic Applications. *Eur. J. Inorg. Chem.* **2012**, 1413-1422.

(81) Hudnall, T. W.; Bielawski, C. W. An N,N'-Diamidocarbene: Studies in C-H Insertion, Reversible Carbonylation, and Transition-Metal Coordination Chemistry. *J. Am. Chem. Soc.* **2009**, *131*, 16039-16040.

(82) César, V.; Lugan, N.; Lavigne, G. Reprogramming of a Malonic N-Heterocyclic Carbene: A Simple Backbone Modification with Dramatic Consequences on the Ligand's Donor Properties. *Eur. J. Inorg. Chem.* **2010**, 361-365.

(83) Hudnall, T. W.; Tennyson, A. G.; Bielawski, C. W. A Seven-Membered N,N'-Diamidocarbene. *Organometallics* **2010**, *29*, 4569-4578.

(84) Blake, G. A.; Moerdyk, J. P.; Bielawski, C. W. Tuning the Electronic Properties of Carbenes: A Systematic Comparison of Neighboring Amino versus Amido Groups. *Organometallics* **2012**, *31*, 3373-3378.

(85) Back, O.; Henry-Ellinger, M.; Martin, C. D.; Martin, D.; Bertrand, G. $^{31}$P NMR Chemical Shifts of Carbene-Phosphinidene Adducts as an Indicator of the π-Accepting Properties of Carbenes. *Angew. Chem. Int. Ed.* **2013,** *52*, 2939-2943.

(86) Chen, M.; Moerdyk, J. P.; Blake, G. A.; Bielawski, C. W.; Lee, J. K. Assessing the Proton Affinities of N,N '-Diamidocarbenes. *J. Org. Chem.* **2013**, *78*, 10452-10458.

(87) Vummaleti, S. V. C.; Nelson, D. J.; Poater, A.; Gómez-Suárez, A.; Cordes, D. B.; Slawin, A. M. Z.; Nolan, S. P.; Cavallo, L. What Can NMR Spectroscopy of Selenoureas and Phosphinidenes Teach Us About the π-Accepting Abilities of N-Heterocyclic Carbenes? *Chem. Sci.* **2015**, *6*, 1895-1904.

(88) Hudnall, T. W.; Moerdyk, J. P.; Bielawski, C. W. Ammonia N-H activation by a N,N'-Diamidocarbene. *Chem. Commun.* **2010**, *46*, 4288-4290.

(89) Perry, L. M. US3476769 (A), 1969.

(90) Stoll, S.; Schweiger, A. EasySpin, A Comprehensive Software Package for Spectral Simulation and Analysis in EPR. *J. Magn. Reson.* **2006**, *178*, 42-55.

(91) Banach, Ł.; Guńka, P. A.; Buchowicz, W., Half-Sandwich Nickel Complexes with Ring-Expanded NHC ligands - Synthesis, Structure and Catalytic Activity in Kumada-Tamao-Corriu Coupling. *Dalton Trans.* **2016**, *45*, 8688-8692.

(92) Collins, L. R.; Riddlestone, I. M.; Mahon, M. F.; Whittlesey, M. K., A Comparison of the Stability and Reactivity of Diamido- and Diaminocarbene Copper Alkoxide and Hydride Complexes. *Chem. Eur. J.* **2015,** *21*, 14075-14084.

(93) One metric per disordered component.

(94) Neese, F. The ORCA Program System. *Wiley Interdiscip. Rev.: Comput. Mol. Sci.* **2012**, *2*, 73-78.

(95) Lee, C. T.; Yang, W. T.; Parr, R. G. Development of the Colle-Salvetti Correlation-Energy Formula into a Functional of the Electron Density. *Phys. Rev. B* **1988**, *37*, 785-789.

(96) Becke, A. D. A New Mixing of Hartree-Fock and Local Density-Functional Theories. *J. Chem. Phys.* **1993**, *98*, 1372-1377.

(97) Becke, A. D. Density-Functional Thermochemistry 3. The Role of Exact Exchange. *J. Chem. Phys.* **1993**, *98*, 5648-5652.

(98) Schafer, A.; Horn, H.; Ahlrichs, R. Fully Optimized Contracted Gaussian-Basis Sets for Atoms Li to Kr. *J. Chem. Phys.* **1992**, *97*, 2571-2577.

(99) Weigend, F.; Ahlrichs, R. Balanced Basis Sets of Split Valence, Triple Zeta Valence and Quadruple Zeta Valence Quality for H to Rn: Design and Assessment of Accuracy. *Phys. Chem. Chem. Phys.* **2005**, *7*, 3297-3305.

(100) Becke, A. D. Density-Functional Exchange-Energy Approximation with Correct Asymptotic-Behavior. *Phys. Rev. A* **1988**, *38*, 3098-3100.

(101) Perdew, J. P. Density-Functional Approximation for the Correlation-Energy of the Inhomogeneous Electron Gas. *Phys. Rev. B* **1986**, *33*, 8822-8824.

(102) Grimme, S.; Ehrlich, S.; Goerigk, L. Effect of the Damping Function in Dispersion Corrected Density Functional Theory. *J. Comput. Chem.* **2011**, *32*, 1456-1465.

(103) Grimme, S.; Antony, J.; Ehrlich, S.; Krieg, H. A Consistent and Accurate Ab Initio Parametrization of Density Functional Dispersion Correction (DFT-D) for the 94 Elements H-Pu. *J. Chem. Phys.* **2010**, *132*, 154104.

(104) Pilbrow, J. *Transition Ion Electron Paramagnetic Resonance*, Clarendon Press, Oxford, **1990**.

(105) Telser, J. Overview of Ligand Versus Metal Centered Redox Reactions in Tetraaza Macrocyclic Complexes of Nickel with a Focus on Electron Paramagnetic Resonance Studies. *J. Braz. Chem. Soc.* **2010**, *21*, 1139-1157.

(106) Kochem, A.; Neese, F.; van Gastel, M. Spectroscopic and Quantum Chemical Study of the $Ni(P^{Ph}{}_2N^{C6H4CH2P(O)(OEt)2}{}_2)_2$ Electrocatalyst for Hydrogen Production with Emphasis on the $Ni^{I}$ Oxidation State. *J. Phys. Chem. C* **2014**, *118*, 2350−2360.

(107) Niklas, J.; Westwood, M.; Mardis, K. L.; Brown, T. L.; Pitts-McCoy, A. M.; Hopkins, M. D.; Poluektov, O. G. X-ray Crystallographic, Multifrequency Electron Paramagnetic Resonance, and Density Functional Theory Characterization of the $Ni(P^{Cy}{}_2N^{tBu}{}_2)_2^{n+}$ Hydrogen Oxidation Catalyst in the Ni(I) Oxidation State. *Inorg. Chem*. **2015**, *54*, 6226-6234.

(108) Nilges, M. J.; Barefield, E. K.; Belford, R. L.; Davis, P. H. Electronic Structure of Three-Coordinate Nickel(I): Electron Paramagnetic Resonance of Nickel-Doped Halobis(triphenylphosphine)copper(I). *J. Am. Chem. Soc.* **1977**, *99*, 755-760.

(109) Saraev, V. V.; Kraikivskii, P. B.; Svoboda, I.; Kuzakov, A. S.; Jordan, R. F. Synthesis, Molecular Structure, and EPR Analysis of the Three-Coordinate Ni(I) Complex $[Ni(PPh_3)_3][BF_4]$. *J. Phys. Chem. A* **2008**, *112*, 12449–12455.

(110) Pietrzyk, P.; Podolska, K.; Sojka, Z. DFT Analysis of **g** and $^{13}C$ Hyperfine Coupling Tensors for Model $Ni^{I}(CO)_nL_m$ ($n$ = 1-4, L = $H_2O$, $OH^-$) Complexes Epitomizing Surface Nickel(I) Carbonyls. *J. Phys. Chem. A* **2008**, *112*, 12208-12219.

(111) Bai, G. C.; Wei, P. R.; Stephan, D. W. A $\beta$-Diketiminato-Nickel(II) Synthon for Nickel(I) Complexes. *Organometallics* **2005**, *24*, 5901-5908.

(112) Eckert, N. A.; Dinescu, A.; Cundari, T. R.; Holland, P. L. A T-Shaped Three-Coordinate Nickel(I) Carbonyl Complex and the Geometric Preferences of Three-Coordinate $d^9$ Complexes. *Inorg. Chem.* **2005**, *44*, 7702-7704.

(113) Holland, P. L.; Cundari, T. R.; Perez, L. L.; Eckert, N. A.; Lachicotte, R. J. Electronically Unsaturated Three-Coordinate Chloride and Methyl Complexes of Iron, Cobalt, and Nickel. *J. Am. Chem. Soc.* **200**2, *124*, 14416-14424.

(114) Ge, P. H.; Riordan, C. G.; Yap, G. P. A.; Rheingold, A. L. A Homoleptic Thioether Coordination Sphere That Supports Nickel(I). *Inorg. Chem.* **1996**, *35*, 5408-5409.

(115) Hoffman, B. M.; Martinsen, J.; Venters, R. A. General-Theory of Polycrystalline ENDOR Patterns - **g** and Hyperfine Tensors of Arbitrary Symmetry and Relative Orientation. *J. Magn. Reson.* **1984**, *59*, 110-123.

(116) Hurst, G. C.; Henderson, T. A.; Kreilick, R. W. Angle-Selected ENDOR Spectroscopy 1. Theoretical Interpretation of ENDOR Shifts from Randomly

Orientated Transition-Metal Complexes. *J. Am. Chem. Soc.* **1985**, *107*, 7294-7299.

(117) Henderson, T. A.; Hurst, G. C.; Kreilick, R. W. Angle-Selected ENDOR Spectroscopy 2. Determination of Proton Coordinates from a Polycrystalline Sample of Bis(2,4-Pentanedionato)Copper(II). *J. Am. Chem. Soc.* **1985**, *107*, 7299-7303.

(118) Murphy, D. M.; Farley, R. D. Principles and Applications of ENDOR Spectroscopy for Structure Determination in Solution and Disordered Matrices. *Chem. Soc. Rev.* **2006**, *35*, 249-268.

(119) Rieger, P. H. Electron Paramagnetic Resonance Studies of Low-Spin $d^5$ Transition Metal Complexes. *Coord. Chem. Rev.* **1994**, *135*, 203-286.

(120) Rudin, M.; Fauth, J. M.; Schweiger, A.; Ernst, R. R.; Zoller, L.; Ammeter, J. H. Spin Density Distribution in Cobaltocene - A Proton ENDOR Study on $Co(Cp)_2$ Diluted in $Mn(Cp)(CO)_3$ Single-Crystals. *Mol. Phys*. **1983**, *49*, 1257-1275.

(121) McDyre, L. E.; Carter, E.; Cavell, K. J.; Murphy, D. M.; Platts, J.; Sampford, K.; Ward, B.; Gabrielli, W. F.; Hanton, M. J.; Smith, D. M. Intramolecular Formation of $Cr^{I}$(bis-arene) Species Via TEA Activation of $[Cr(CO)_4(Ph_2P(C_3H_6)PPh_2)]^+$; An EPR and DFT Investigation. *Organometallics* **2011**, *30*, 4505-4508.

**Table 1.** Data Collection and Refinement Details for the Crystal Structures of **1-3.**

| Identification code | **1** | **2** | **3** |
|---|---|---|---|

| | | | |
|---|---|---|---|
| Empirical formula | $C_{27}H_{33}N_2Ni$ | $C_{28}H_{35}N_2Ni$ | $C_{29}H_{33}N_2NiO_2$ |
| Formula weight | 444.26 | 458.29 | 500.28 |
| Crystal system | monoclinic | triclinic | orthorhombic |
| Space group | $P2_1/n$ | $P$-1 | $Pbcn$ |
| $a$/Å | 9.0299(2) | 9.0066(3) | 26.0692(4) |
| $b$/Å | 30.5459(7) | 9.4373(3) | 9.07493(17) |
| $c$/Å | 9.5199(2) | 15.9678(5) | 21.6239(4) |
| $\alpha$/° | 90 | 100.212(3) | 90 |
| $\beta$/° | 117.041(3) | 93.339(3) | 90 |
| $\gamma$/° | 90 | 113.601(3) | 90 |
| $U$/Å$^3$ | 2338.79(12) | 1211.38(7) | 5115.70(16) |
| $Z$ | 4 | 2 | 8 |
| $\rho_{calc}$/gcm$^{-3}$ | 1.262 | 1.256 | 1.299 |
| $\mu$/mm$^{-1}$ | 1.292 | 1.262 | 1.305 |
| F(000) | 948.0 | 490.0 | 2120.0 |
| Crystal size/mm$^3$ | 0.2044 × 0.1321 × 0.0817 | 0.194 × 0.0941 × 0.0862 | 0.1192 × 0.0946 × 0.0612 |
| 2θ range for data collection/° | 10.828 to 143.898 | 10.778 to 144.074 | 8.178 to 143.998 |
| Index ranges | $-10 \le h \le 11$,<br>$-35 \le k \le 37$,<br>$-11 \le l \le 10$ | $-11 \le h \le 11$,<br>$-9 \le k \le 11$,<br>$-19 \le l \le 19$ | $-24 \le h \le 32$,<br>$-10 \le k \le 11$,<br>$-26 \le l \le 25$ |
| Reflections collected | 14915 | 11545 | 25391 |
| Independent reflections, $R_{int}$ | 4567, 0.0345 | 4745, 0.0210 | 5016, 0.0378 |
| Data/restraints/parameters | 4567/0/277 | 4745/0/286 | 5016/0/324 |
| Final $R1$, $wR2$ [I>=2σ (I)] | 0.0365, 0.0939 | 0.0358, 0.0931 | 0.0372, 0.0982 |
| Final $R1$, $wR2$ [all data] | 0.0409, 0.0979 | 0.0377, 0.0947 | 0.0483, 0.1052 |
| Largest diff. peak/hole / e Å$^{-3}$ | 0.58/-0.28 | 0.79/-0.44 | 0.31/-0.33 |

**Table 3**. Experimental and DFT-calculated principal *g* spin Hamiltonian parameters for the CpNi(RE-NHC) complexes **1**-**3**.

| **Compound** | | ***g* values** | | | | **Ref** |
|---|---|---|---|---|---|---|
| | | $g_1$ | $g_2$ | $g_3$ | $g_{iso}$ | |
| **1** | Exp | 2.052 | 2.204 | 2.324 | 2.193 | t.w. |
| | DFT | 2.082 | 2.180 | 2.255 | 2.172 | |
| **2** | Exp | 2.052 | 2.154 | 2.313 | 2.17 | t.w. |
| | DFT | 2.082 | 2.132 | 2.244 | 2.153 | |
| **3** | Exp | 2.032 (*2.054*) | 2.095 (*2.076*) | 2.262 (*2.262*) | 2.130 *(2.131)* | t.w. |
| | DFT | 2.054 (*2.058*) | 2.202 (*2.150*) | 2.241 (*2.240*) | 2.166 *(2.149)* | |
| **D1**[1] | | 2.377 | 2.306 | 2.050 | | 51,52 |
| **D1**[1] | | 2.362 | 2.306 | 2.049 | | 53 |
| **D1**[2] | | 2.349 | 2.267 | 2.062 | | 53 |
| **E** | | 2.405-2.275 | 2.322-2.216 | 2.073-2.034 | | 71 |

Note: The *g* values are quoted ± 0.003; $g_{iso} = (g_1+g_2+g_3)/3$. The Euler rotation of the **g** tensor, defined with respect to the molecular frame = 32±1°, 82±1°, 162±1° for (**1**-**3**). For CpNi(6-MesDAC) (**3**), two Ni(I) centers were identified from the VT EPR spectra, labelled Ni1 and Ni1b (the *g* values for the latter are given in italics). [1]NHC = imidazol-2-ylidene. [2]NHC = imidazolin-2-ylidene. See Scheme 1 for structures of **D1** and **E**.

**Table 4**. Experimental and DFT-calculated principal $^1$H hyperfine spin Hamiltonian parameters for the CpNi(RE-NHC) complexes **1**-**3**.

| **Compound** | | **Cp proton** | ***A* values (MHz)** | | | | **Euler angles for *A* (°)** | | |
|---|---|---|---|---|---|---|---|---|---|
| | | | $A_1$ | $A_2$ | $A_3$ | $a_{iso}$ | α | β | γ |
| **1** | Exp | $H_{large}$ | -3.7 | -9.1 | -10.9 | -5.4 | 32 | 94 | 183 |
| | | $H_{small}$ | -2.3 | -3.4 | 6.8 | 0.4 | 16 | 85 | -158 |
| | DFT | H9 ($H_{large}$) | 4.7 | -5.5 | -7.4 | -2.7 | | | |
| | | H10 ($H_{large}$) | 4.0 | -6.0 | -9.8 | -3.9 | | | |
| | | H8 ($H_{small}$) | -2.6 | -3.4 | 6.8 | 0.3 | | | |
| | | H11($H_{small}$) | -2.8 | -3.9 | 6.0 | -0.2 | | | |
| **2** | Exp | $H_{large}$ | 3.9 | -6.4 | -11.2 | -4.6 | 32 | 94 | 183 |
| | | $H_{small}$ | -2.3 | -3.4 | 6.8 | 0.4 | 16 | 85 | -158 |
| | DFT | H2 ($H_{large}$) | 3.9 | -6.4 | -10.5 | -4.3 | | | |
| | | H13 ($H_{large}$) | 4.9 | -5.3 | -6.6 | -2.3 | | | |
| | | H3 ($H_{small}$) | -2.1 | -5.7 | 6.7 | -0.4 | | | |
| | | H8 ($H_{small}$) | -2.8 | -4.0 | 6.8 | 0.0 | | | |
| **3** | Exp | $H_{large}$ | 3.0 | -8.6 | -13.3 | -6.3 | 32 | 96 | 183 |
| | | $H_{small}$ | -4.7 | 6.8 | -7.6 | -1.8 | 16 | 85 | -158 |
| | DFT | H10 ($H_{large}$) | 3.3 | -6.8 | -12.1 | -5.2 | 32 | 97 | 171 |
| | | H11 ($H_{large}$) | 3.8 | -6.1 | -10.2 | -4.2 | 45 | 64 | 101 |
| | | H7 ($H_{small}$) | -4.7 | 6.8 | -7.0 | -1.7 | 16 | 85 | -158 |
| | | H9 ($H_{small}$) | -4.7 | 6.3 | -6.6 | -1.7 | -34 | 92 | -101 |

Note: The *A* values are quoted ± 0.1 MHz; $A_{iso} = (A_1+A_2+A_3)/3$. $H_{large}$ = large proton couplings, $H_{small}$ = small proton couplings, from the Cp ring. The labelled protons responsible for $H_{large}$ and $H_{small}$ given in the table are numbered as in the geometry optimized crystal structure used to perform the DFT calculation to obtain **g** and **A** tensors. The Euler rotation of the **A** tensor, is defined with respect to the molecular frame, with values given in degrees for **1**-**3**.

*Table of Contents Synopsis*

Continuous wave X-/Q-band EPR and Q-band $^{1}$H ENDOR spectroscopy, in combination with computational methods, has been used to probe the electronic structure of the paramagnetic half-sandwich Ni(I) ring-expanded diamino/diamidocarbene complexes CpNi(RE-NHC) (RE-NHC = 6-Mes, 7-Mes, 6-MesDAC).

*For Table of Contents Only*